

# CloudMamba: Grouped Selective State Spaces for Point Cloud Analysis

Kanglin Qu<sup>1</sup>, Pan Gao<sup>1\*</sup>, Qun Dai<sup>1\*</sup>, Zhanzhi Ye<sup>1</sup>, Rui Ye<sup>2</sup>, Yuanhao Sun<sup>3</sup>

<sup>1</sup>College of Artificial Intelligence, Nanjing University of Aeronautics and Astronautics, Nanjing, 211106, China

<sup>2</sup>College of Artificial Intelligence, Nanjing Agricultural University, Nanjing, 210095, China

<sup>3</sup>School of Mathematical Sciences, Beijing University of Posts and Telecommunications, Beijing 100876, China  
klinqu@163.com, {Pan.Gao, daiqun, yezhanzhi}@nuaa.edu.cn, yerui@njau.edu.cn, sunyh@bupt.edu.cn

## Abstract

Due to the long-range modeling ability and linear complexity property, Mamba has attracted considerable attention in point cloud analysis. Despite some interesting progress, related work still suffers from imperfect point cloud serialization, insufficient high-level geometric perception, and overfitting of the selective state space model (S6) at the core of Mamba. To this end, we resort to an SSM-based point cloud network termed CloudMamba to address the above challenges. Specifically, we propose sequence expanding and sequence merging, where the former serializes points along each axis separately and the latter serves to fuse the corresponding higher-order features causally inferred from different sequences, enabling unordered point sets to adapt more stably to the causal nature of Mamba without parameters. Meanwhile, we design chainedMamba that chains the forward and backward processes in the parallel bidirectional Mamba, capturing high-level geometric information during scanning. In addition, we propose a grouped selective state space model (GS6) via parameter sharing on S6, alleviating the overfitting problem caused by the computational mode in S6. Experiments on various point cloud tasks validate CloudMamba’s ability to achieve state-of-the-art results with significantly less complexity.

## Code —

<https://github.com/Point-Cloud-Learning/CloudMamba>

## Proceedings version —

[https://ojs.aaai.org/index.php/AAAI/article/view/\\*\\*\\*\\*\\*](https://ojs.aaai.org/index.php/AAAI/article/view/*****)

## Introduction

The attention mechanism (Vaswani et al. 2017; Dosovitskiy et al. 2021) is gradually replacing the convolution as a dominant operator in point cloud analysis with its ability to achieve global modeling, but its quadratic complexity causes unbearable computational overheads. To handle this challenge, existing attention-based networks (Nie et al. 2022; Fan et al. 2022; Park et al. 2022; Liu et al. 2023) perform attention interactions in local neighborhoods or within windows, which, however, impose constraints on receptive fields. Recently, state space models (SSMs) (Gu et al. 2021;

\*Corresponding author.

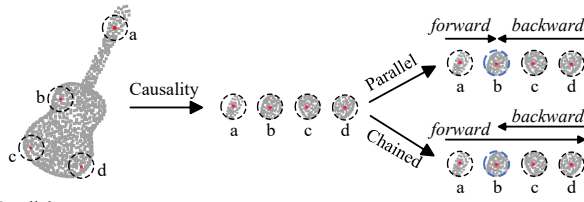
Serialization	Grid size	OA (%)
Hilbert + Trans-Hilbert	0.010	90.84
Hilbert + Trans-Hilbert	0.015	92.82
Hilbert + Trans-Hilbert	0.020	89.13
Sequence expanding & merging	/	<b>93.65</b>

Table 1: Experimental results of different serialization methods in our network on ModelNet40 dataset.

Gu, Goel, and Ré 2022; Mehta et al. 2022; Gupta, Gu, and Berant 2022) have shown great potential in natural language processing (NLP). Mamba (Gu and Dao 2023) achieves flexible selection of relevant information in a data-dependent manner by the selective state space model (S6), further enhancing long-range modeling capability. Moreover, Mamba with linear complexity adopts a hardware-aware algorithm inspired by FlashAttention (Dao et al. 2022), significantly improving training and inference efficiencies.

Given Mamba’s success in NLP, some works (Han et al. 2024; Liang et al. 2024b; Liu et al. 2024a; Zhang et al. 2024) attempt to transplant this success from language modeling to point cloud analysis. In this process, despite some significant progress, these efforts still struggle to achieve satisfactory results due to the following three aspects:

- **Point cloud serialization.** It is crucial to build inter-point structure dependencies in a point sequence by serialization for Mamba’s causal inference, and existing strategies are mostly based on space-filling curves. However, the reliability of the structural dependencies built by space-filling curves is highly sensitive to the setting of the grid size, as shown in Tab. 1. Besides, as a pioneering study based on Mamba, PointMamba (Liang et al. 2024b) concatenates the serialization results of the Hilbert curve and its variant Trans-Hilbert (Hilbert 1935). However, this practice has the following shortcomings: (1) a longer sequence induced by the concatenation introduces redundancy and negatively affects efficiency, and (2) concatenating serialized sequences with different spatial relationships tends to cause confusion. Hence, existing efforts are imperfect in point cloud serialization.
- **High-level geometric perception.** While Mamba achieves superior long-range modeling via the selection mechanism, it is only unidirectional and not applicable



Parallel structure:

$$\begin{cases} \text{biMamba}^p(a) = \text{forward}(a) + \text{backward}(a) = \text{SSM}(a) + \text{SSM}(d, c, b, a) \\ \text{biMamba}^p(b) = \text{forward}(b) + \text{backward}(b) = \text{SSM}(a, b) + \text{SSM}(d, c, b) \\ \text{biMamba}^p(c) = \text{forward}(c) + \text{backward}(c) = \text{SSM}(a, b, c) + \text{SSM}(d, c) \\ \text{biMamba}^p(d) = \text{forward}(d) + \text{backward}(d) = \text{SSM}(a, b, c, d) + \text{SSM}(d) \end{cases}$$

Chained structure:

$$\begin{cases} \text{forward}(a) = \text{SSM}(a) = \hat{a} \\ \text{forward}(b) = \text{SSM}(a, b) = \hat{b} \\ \text{forward}(c) = \text{SSM}(a, b, c) = \hat{c} \\ \text{forward}(d) = \text{SSM}(a, b, c, d) = \hat{d} \end{cases} \quad \begin{cases} \text{biMamba}^c(a) = \text{backward}(a) = \text{SSM}(\hat{d}, \hat{c}, \hat{b}, \hat{a}) \\ \text{biMamba}^c(b) = \text{backward}(b) = \text{SSM}(\hat{d}, \hat{c}, \hat{b}) \\ \text{biMamba}^c(c) = \text{backward}(c) = \text{SSM}(\hat{d}, \hat{c}) \\ \text{biMamba}^c(d) = \text{backward}(d) = \text{SSM}(\hat{d}) \end{cases}$$

Figure 1: Inference process of the bidirectional Mamba with different structures, where the blue equations denote the inference processes of both bidirectional Mamba for the point  $b$ , respectively. In the backward inference of the chained structure, the previous points perceive the high-level structural semantics that are inferred from the forward Mamba.

to visual data requiring global learning. Therefore, some works (Liu et al. 2024a; Zhang et al. 2024) introduce the bidirectional Mamba with a parallel structure from Vision Mamba (Zhu et al. 2024). However, this structure limits the expressivity of networks. As illustrated in Fig. 1, the parallel bidirectional Mamba provides each point with a global receptive field through the forward and backward inference, *e.g.*, the point  $b$  can interact with  $a$ ,  $c$ , and  $d$ . Nevertheless, we argue that this type of inference on primitive low-order geometric features can result in insufficient high-level geometric perception.

- **Computational mode in S6.** Existing Mamba-based point cloud works (Liang et al. 2024b; Liu et al. 2024a; Zhang et al. 2024) take S6 as the core component, where each dimension is learned by a separate set of parameters when dealing with multi-dimensional sequences, as shown in Fig. 2(a). This computational mode results in overfitting in causal inference due to excessive parameters in each dimension.

According to the above analyses, we propose a novel SSM-based point cloud network termed CloudMamba, which obeys the following designs to address the above challenges encountered in related works in order to greatly promote the development of Mamba in the point cloud domain:

- **Sequence expanding & merging.** We propose sequence expanding, which serializes points along each axis separately, and sequence merging, which fuses the corresponding higher-order features causally inferred from different sequences. The sequence expanding directly builds structural dependencies in multiple perspectives from different axes, which not only overcomes the parameter sensitivity in space-filling curves, but also avoids the inefficiency and causal confusion caused by concatenating different serialization results. Furthermore, it

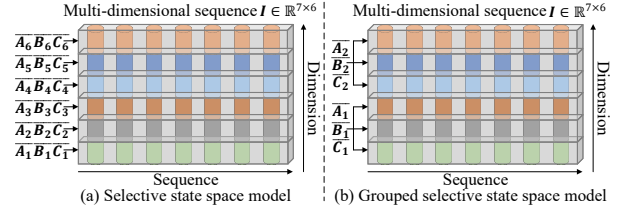


Figure 2: Computational modes of S6 and GS6, where GS6’s grouping rate is 3. A multi-dimensional sequence  $I \in \mathbb{R}^{7 \times 6}$  is used as an example, with the subscript denoting the parameter to be used for a dimension or a set of dimensions.

captures rich geometric information by integrating with the sequence merging. Together, these enable unordered point sets to adapt more stably to the causal nature of Mamba without parameters, as shown in Tab. 1.

- **ChainedMamba.** We propose a chained bidirectional Mamba termed chainedMamba, which chains the forward and backward processes in the parallel bidirectional Mamba. In this case, due to the chaining property, the point  $b$  could interact with the high-level structural semantics of  $d$ ,  $c$ ,  $b$ , *i.e.*,  $\hat{d}$ ,  $\hat{c}$ , and  $\hat{b}$  as shown in Fig. 1. By utilizing these high-level structural semantics inferred from low-order geometric features in the forward Mamba during backward inference, it can achieve superior high-level geometric perception, as demonstrated in Tab. 7.
- **GS6.** We propose a grouped selective state space model (GS6) by sharing a same set of parameters across several dimensions, which alleviates the overfitting caused by the computational mode in S6, as illustrated in Fig. 2(b).

Finally, we conduct experiments on point cloud recognition ModelNet40 (Wu et al. 2015) and ScanObjectNN (Uy et al. 2019), part segmentation ShapeNet (Yi et al. 2016), as well as semantic segmentation S3DIS (Armeni et al. 2016). Experimental comparisons show CloudMamba is able to obtain state-of-the-art accuracy with linear complexity.

In summary, the contributions of this paper are fourfold:

- (1) A novel SSM-based point cloud network, CloudMamba, is constructed upon Mamba, which achieves state-of-the-art results in various point cloud tasks with linear complexity.
- (2) A serialization method consisting of sequence expanding and sequence merging is proposed, which builds structural dependencies directly from the coordinate axes defining spatial locations and captures rich geometric information by merging the sequences generated along different axes, making unordered point sets better adapted to the causal nature of Mamba without parameters.
- (3) A chained bidirectional Mamba termed chainedMamba is designed by chaining the forward and backward processes in the parallel bidirectional Mamba. This simple yet effective refinement achieves excellent high-level geometric perception.
- (4) A variant GS6 on S6 is proposed by adopting the parameter sharing, which mitigates overfitting in S6. To our best knowledge, all existing Mamba-based methods are based on

S6, and GS6 is the first exploration of optimizing the computational mode in S6.

## Related work

### SSMs and Mamba

SSMs are mathematical models used in control theory to describe dynamic systems, which have recently been introduced to deep learning and have been developed considerably in long sequence modeling. Initially, Gu *et al.* (Gu et al. 2021) designed a linear state space layer (LSSL) based on linear continuous-time state space representations and demonstrated its potential to deal with long-range dependencies in sequential data by combining it with the HiPPO initialization (Gu et al. 2020). However, LSSL requires excessive computational resources and cannot be used as a generic sequential modeling method. Hence, the structured state space sequence model (S4) (Gu, Goel, and Ré 2022) normalizes the parameters into a diagonal structure to solve the computational bottleneck. Subsequently, many efforts have been made to improve SSMs, such as GSS (Mehta et al. 2022), S5 (Smith, Warrington, and Linderman 2022), and DSS (Gupta, Gu, and Berant 2022), among which S6 is a landmark work, featuring a selective scanning mechanism and linear complexity. To enable flexible integration into neural networks, S6 is combined with the simplified H3 architecture (Gu and Dao 2023) to build Mamba, which achieves impressive results in NLP. Later, several works extend Mamba to other research directions, including image recognition (Liu et al. 2024b, 2025), medical image segmentation (Ruan and Xiang 2024; Ma, Li, and Wang 2024), and graph sequence modeling (Wang et al. 2024a).

Recently, Mamba has also begun to be applied to point cloud analysis. Mamba3D (Han et al. 2024) focuses on enhancing local features using Mamba, but it does not take into consideration the unidirectional modeling property of Mamba as our network does. PointMamba (Liang et al. 2024b) and OctMamba (Liu et al. 2024a) employ space-filling curves to form causal sequences for Mamba. Different from them, our network directly adopts coordinate axes to build structural dependencies in multiple perspectives without parameters, overcoming the parameter sensitivity in space-filling curves. PCM (Zhang et al. 2024) employs the parallel bidirectional Mamba, resulting in insufficient high-level geometric perception. In our work, chained-Mamba achieves excellent high-level geometric perception by chaining the forward and backward processes in the parallel bidirectional Mamba. Finally, all the previous works only apply directly Mamba to point cloud analysis, while we improve its S6 to mitigate potential overfitting.

## Preliminaries

### SSMs

SSMs are cyclic processes with latent states, which map a 1-D equation or sequence  $x(t) \in \mathbb{R}^N$  to  $y(t) \in \mathbb{R}^N$  by a latent state  $h(t) \in \mathbb{R}^N$ . The process is mathematically denoted as a linear ordinary differential equation as follows

$$y(t) = Ch(t), h'(t) = Ah(t) + Bx(t), \quad (1)$$

where the three parameters  $A \in \mathbb{R}^{N \times N}$ ,  $B \in \mathbb{R}^N$ , and  $C \in \mathbb{R}^N$  represent the state matrix, input matrix, and output matrix, respectively. Since the above SSMs run on continuous inputs and are not applicable to discrete inputs such as images and text, they cannot be introduced into deep models. Thus, it is necessary to discretize them, and the zero-order hold is commonly used as a discretization method (see Appendix A). The discretized formulas are as follows

$$y_t = \bar{C}h_t, \quad h_t = \bar{A}h_{t-1} + \bar{B}x_t, \quad (2)$$

where  $\bar{A}$  and  $\bar{B}$  are the results of discretizing the continuous parameters  $A$  and  $B$  by a time scale  $\Delta$ , denoted as

$$\bar{A} = e^{\Delta A}, \quad \bar{C} = C, \quad \bar{B} = (\Delta A)^{-1}(e^{\Delta A} - I)(\Delta B). \quad (3)$$

### Mamba

Since processing the input and latent state equally, previous approaches focusing on linear time-invariant SSMs (where  $\bar{A}$  and  $\bar{B}$  are invariant) may fail to capture critical information from context. Therefore, Mamba proposes a novel SSM (termed S6) by integrating an input-dependent selective mechanism into SSMs, where  $\bar{A}$  and  $\bar{B}$  are the functions of inputs, indicating Mamba is linear time-variant.

However, Mamba’s linear time-variant parameters result in dynamic weights, preventing it from being computed as efficiently as linear time-invariant SSMs using the convolution. Thus, Mamba uses a parallel scanning algorithm with linear complexity (Smith, Warrington, and Linderman 2022; Martin and Cundy 2018) to maintain efficient computation. In addition, it designs a hardware-aware algorithm by utilizing the fast SRAM in GPUs to improve efficiency.

## CloudMamba

### Overview

Figure 3 presents the overview of our network, which takes as input a point set  $P = \{p_i = (c_i, f_i)\}_{i=1}^L$ , where  $c_i \in \mathbb{R}^3$  and  $f_i \in \mathbb{R}^G$  denote the 3D coordinates of  $p_i$  and other relevant features, respectively. In the initial stage,  $P$  is transformed into a high-dimensional space with  $H$  dimensions through an embedding layer consisting of a multi-layer perceptron machine (MLP). Then, an encoder-decoder architecture built on up- and down-sampling layers and hexa-orientation Mamba blocks is used for hierarchical feature aggregation. Finally, a corresponding task head is applied. In this paper, our network is validated by recognition and segmentation results on point clouds. The recognition head processes the output of the encoder through an average pooling layer and an MLP, and the segmentation head employs an MLP to process the output of the decoder. Next, we describe components in the encoder-decoder architecture in detail.

### Hexa-orientation Mamba block

The hexa-orientation Mamba block is the main feature aggregation module of our network, capable of facilitating geometry perception from multiple perspectives, and is used for features at each level to capture fine-grained structures, specifically consisting of sequence expanding, chainedMamba, and sequence merging.

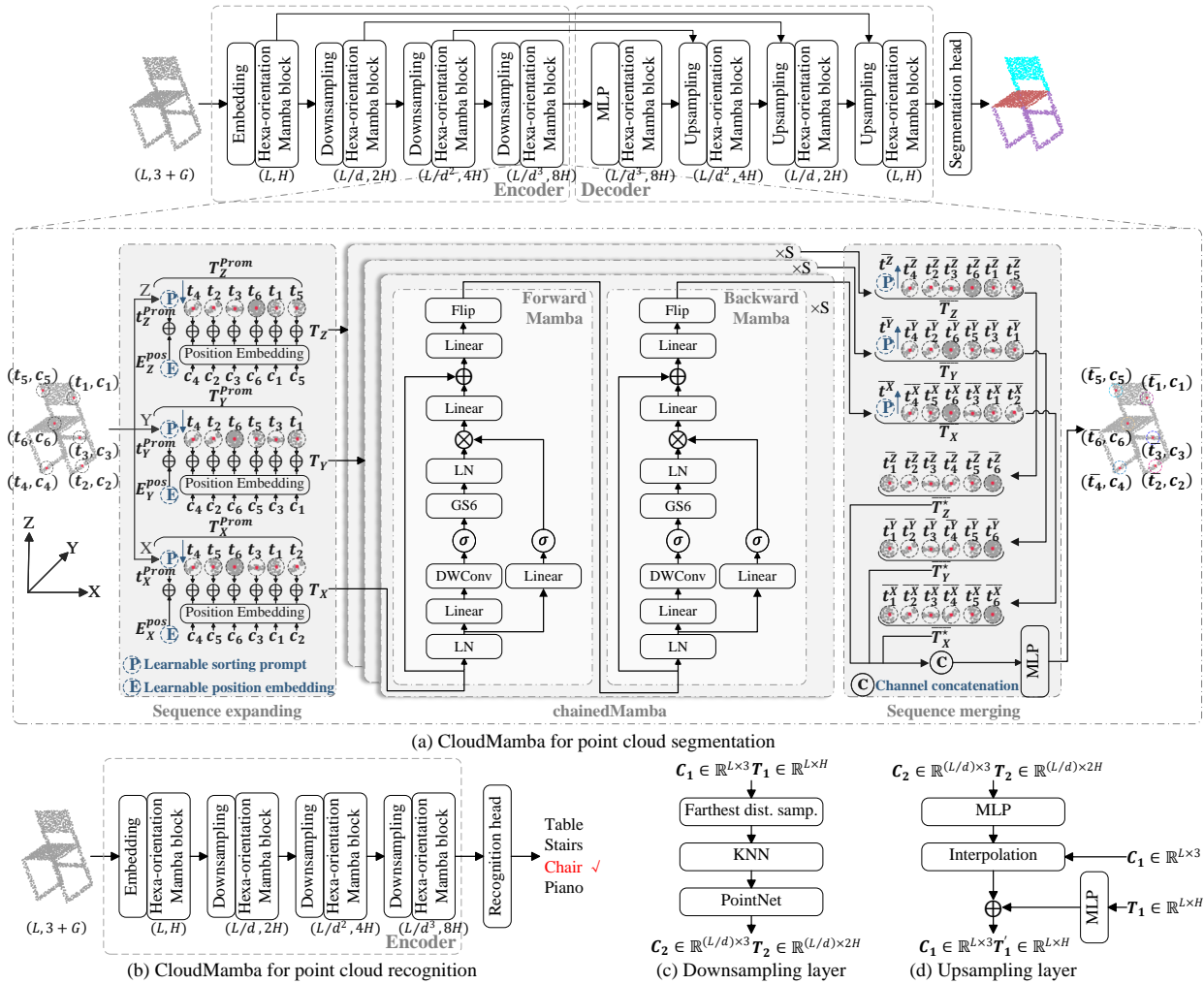


Figure 3: Pipeline of our proposed network. The Flip layer in the chainedMamba indicates a flip operation on the sequence for global modelling. S6 in Mamba is replaced by GS6. Since each point sequence is processed with forward and backward directions, there are hexa orientations for causal modeling.

### Sequence expanding

Mamba tailored for causal sequences requires causal dependencies between elements, but visual data has a non-causal nature, such that applying Mamba directly to point clouds does not achieve expected results (see Tab. 6). Existing strategies mostly build structural dependencies based on the spatial proximity of space-filling curves, yet their reliability is highly sensitive to the setting of the grid size. Hence, we build structural dependencies directly from the coordinate axis defining spatial locations. Since structural dependencies on only one axis cannot reflect rich geometric information, we construct causal sequences based on the ascending order of point coordinates  $C = \{c_1, c_2, \dots, c_j\}$  corresponding to input point features  $T = \{t_1, t_2, \dots, t_j\}$  along the Z, Y, and X axes, respectively

$$T_A^{Cau} = \{t_{A_1}, t_{A_2}, \dots, t_{A_j}\} \quad A \in \{Z, Y, X\}, \quad (4)$$

where  $T_A^{Cau}$  denotes a causal sequence constructed on the A-axis,  $t_{A_j}$  represents the  $j$ -th point feature sorted on the

A-axis, and  $A_j$  corresponds to a subscript in  $T$ .

**Prompt.** Since the network involves the structural dependencies arising from three different directions (these causal sequences are essentially shared, differing only in sorting), a learnable sorting prompt  $t_A^{Prom}$  is added for each sequence to avoid confusing the network about these dependencies

$$T_A^{Prom} = \{t_A^{Prom}, t_{A_1}, t_{A_2}, \dots, t_{A_j}\}, \quad (5)$$

where  $t_A^{Prom}$  is a sorting prompt added for the A axis.

**Position-aware.** Visual data is location-sensitive (Zhao et al. 2021). While point coordinates contain position information, fine-grained position information may be lost in higher-level features as the network deepens. Additionally, unlike the convolution, SSMs cannot implicitly endow the network with the spatial inductive bias. Thus, we explicitly provide position information to corresponding point features by position embeddings on point coordinates as follows

$$T_A = \{t_A^{Prom} + E_A^{Pos}, t_{A_1} + \rho(c_{A_1}), \dots, t_{A_j} + \rho(c_{A_j})\}, \quad (6)$$

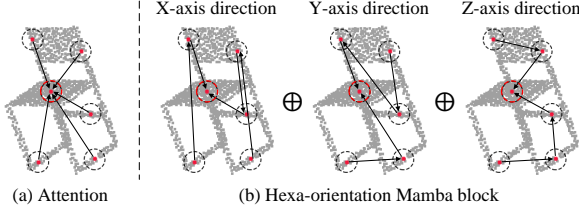


Figure 4: Illustration of the global receptive fields of the attention mechanism and hexa-orientation Mamba block, with the point in the red box as an example.

where  $E_A^{pos}$  is a learnable position embedding we add for each sorting prompt,  $c_{A_j}$  is a point coordinate corresponding to the point feature  $t_{A_j}$ , and  $\rho$  is an MLP used to map point coordinates to position embeddings.

### ChainedMamba

Although the mainstream parallel bidirectional Mamba overcomes the limitation of Mamba for visual data requiring global learning, its inference on primitive low-order geometric features leads to insufficient high-level geometric perception. Therefore, we propose chainedMamba by chaining the forward and backward processes in the parallel bidirectional Mamba, ingeniously realizing superior high-level geometric perception, as shown in Fig. 3. Besides, by combining the causal sequences formed by the sequence expanding, Fig. 4 demonstrates that the hexa-orientation Mamba block is able to facilitate geometric learning from multiple perspectives with a global receptive field, in which the global receptive field is obtained through compressing the historical hidden state in both forward and backward directions, unlike the attention mechanism whereas the global receptive field is obtained through interactions with all elements. Although the way to obtain both global receptive fields is different, there is a close correlation between Mamba and self-attention, *i.e.*, S6 is a special causal self-attention, see Appendix B.

**GS6.** As shown in Eq. 1, SSMs are sequence mappings from  $\mathbb{R}^N \rightarrow \mathbb{R}^N$  on a 1-D sequence, thus S6 uses a separate set of parameters for each dimension when the input sequence has multiple dimensions, which leads to overfitting in causal inference due to excessive parameters in each dimension (see Tab. 5). To improve the generalizability of the network, we propose a grouped selective state space model (GS6) through parameter sharing on S6, as shown in Algorithm 1, where  $\text{Linear}_N$  denotes a linear layer projected to dimension  $N$  and  $\text{Repeat}(\mathbf{V}, g)$  denotes repeating an element in tensor  $\mathbf{V}$   $g$  times. GS6 uses a grouping ratio  $g$  to make every  $g$  dimensions in  $\mathbf{x}$  using the same set of parameters, alleviating the overfitting caused by S6’s computational mode, while the repeating function ensures the least modification on S6’s coding.

### Sequence merging

After the chainedMamba process different causal sequences  $\{\mathbf{T}_A, A \in \{Z, Y, X\}\}$ , these sequences  $\left(\{\overline{\mathbf{T}}_A = \{t_{A_1}^A, t_{A_2}^A, \dots, t_{A_j}^A\}\}\right)$  contain the higher-order interaction features causally inferred from different

---

### Algorithm 1 S6 + Grouping (GS6)

---

**Input:**  $\mathbf{x}: (B, L, D)$  and a grouping rate  $g$

**Output:**  $\mathbf{y}: (B, L, D)$

1.  $\mathbf{B}: (B, L, N) \leftarrow \text{Linear}_N(\mathbf{x})$

2.  $\mathbf{C}: (B, L, N) \leftarrow \text{Linear}_N(\mathbf{x})$

/\* shape of  $\text{Parameter}_\Delta$  is  $(D/g)$ , and the softplus ensures positive  $\Delta$  \*/

3.  $\Delta: (B, L, D/g) \leftarrow \log\left(1 + e^{(\text{Linear}_{D/g}(\mathbf{x}) + \text{Parameter}_\Delta)}\right)$

/\* shape of  $\text{Parameter}_A$  is  $(D/g, N)$ . Each dimension in  $\mathbf{A}$  represents a structured diagonal  $N \times N$  matrix \*/

4.  $\overline{\mathbf{A}}: (B, L, D/g, N) \leftarrow \Delta \otimes \text{Parameter}_A$

5.  $\overline{\mathbf{B}}: (B, L, D/g, N) \leftarrow \Delta \otimes \mathbf{B}$

6.  $\overline{\mathbf{A}}, \overline{\mathbf{B}}: (B, L, D, N) \leftarrow \text{Repeat}(\overline{\mathbf{A}}, g), \text{Repeat}(\overline{\mathbf{B}}, g)$

/\* time-variant: calculated by the parallel scanning \*/

7.  $\mathbf{y}: (B, L, D) \leftarrow \text{SSM}(\overline{\mathbf{A}}, \overline{\mathbf{B}}, \mathbf{C})(\mathbf{x})$

return  $\mathbf{y}$

---

perspectives, respectively, and the sequence merging is responsible for integrating them together to captures rich geometric information. Specifically, the sorting prompts (the first term) in the sequences are first removed and the sequences are returned to their original order  $\left(\{\overline{\mathbf{T}}_A^* = \{t_1^A, t_2^A, \dots, t_j^A\}\}\right)$ , and then the sequences are merged by Eq. 7, where  $\text{Concat}$  denotes channel-wise concatenation on the corresponding element and  $\gamma$  is an MLP scaled down by three times, keeping the output dimension of the hexa-orientation Mamba block the same as the input dimension.

$$\text{Output} = \gamma(\text{Concat}(\{\overline{\mathbf{T}}_A^*, A \in \{Z, Y, X\}\})) \quad (7)$$

### Downsampling and upsampling layers

**Downsampling.** The downsampling layer is to reduce the cardinality of point sets at a downsampling rate in the encoder. Assume that the input point coordinate set and its corresponding point feature set of the downsampling layer are  $\mathbf{C}_1 \in \mathbb{R}^{L \times 3}$  and  $\mathbf{T}_1 \in \mathbb{R}^{L \times H}$ , respectively, and the downsampling rate is  $d$ . First, the farthest distance sampling (Qi et al. 2017b) is performed in  $\mathbf{C}_1$  to determine a point coordinate subset  $\mathbf{C}_2 \in \mathbb{R}^{(L/d) \times 3}$  with  $L/d$  sampled points. Then, to pool the point features on  $\mathbf{C}_1$  to  $\mathbf{C}_2$ , we perform the  $K$ -nearest neighbor on  $\mathbf{C}_1$  for each point coordinate in  $\mathbf{C}_2$  and pass the neighboring point features of each point in  $\mathbf{C}_2$  through PointNet (Qi et al. 2017a) to construct a point feature set  $\mathbf{T}_2 \in \mathbb{R}^{(L/d) \times 2H}$  corresponding to  $\mathbf{C}_2$ . The overview of the downsampling layer is shown in Fig. 3(c).

**Upsampling.** For dense tasks such as point cloud segmentation, we follow the U-Net design (Ronneberger, Fischer, and Brox 2015), where the above encoder is coupled with a symmetric decoder. The upsampling layer serves as a connection between successive stages in the decoder, and it is to recover the cardinality of point sets according to the corresponding encoder stage. Suppose that the input point coordinate set and its corresponding point feature set of the upsampling layer are  $\mathbf{C}_2 \in \mathbb{R}^{(L/d) \times 3}$  and  $\mathbf{T}_2 \in \mathbb{R}^{(L/d) \times 2H}$ , respectively, and the point coordinate set and its point feature set of the corresponding encoder stage are  $\mathbf{C}_1 \supset \mathbf{C}_2$  ( $\mathbf{C}_1 \in \mathbb{R}^{L \times 3}$ ) and  $\mathbf{T}_1 \in \mathbb{R}^{L \times H}$ , respectively. First, the dimension

of  $T_2$  is aligned to  $T_1$  by an MLP (*i.e.*,  $T_2 \in \mathbb{R}^{(L/d) \times H}$ ), and the tri-linear interpolation method is performed on  $C_2$  for each point in  $C_1$  to obtain the interpolated point features corresponding to  $C_1$  from  $T_2$ . Then,  $T_1$  passing through an MLP is summed with these interpolated point features by the skip connection to obtain a point feature set  $T'_1 \in \mathbb{R}^{L \times H}$  corresponding to  $C_1$  at the decoder stage. Fig. 3(d) illustrates the structure of the upsampling layer.

## Experiment

To validate CloudMamba’s potential in point cloud analysis, it is compared with different types of networks on ModelNet40, ScanObjectNN, ShapeNet, and S3DIS datasets. For a detailed introduction on datasets and evaluation metrics, see Appendix C. Moreover, we explore the network property and the impact of the components on the performance by extensive ablation comparisons. Also, the FLOPs (floating point operations) and Params reported, reflecting computation and space complexity, respectively, are measured on the same RTX 4090 GPU to ensure a fair comparison.

### Point cloud recognition

Table 2 compares the experimental results of our network and different operators-based mainstream works on ModelNet40 dataset. As shown in the fifth column in Tab. 2, CloudMamba achieves a higher OA compared to the concurrent SSM-based works, which indicates that our network is able to take full advantage of Mamba’s superior long-range modeling. Besides, CloudMamba achieves competitive accuracy with the state-of-the-art Point Transformer but consuming less computational resources, which not only stresses the strong geometric representation capability of our network, but also proves it improves computational efficiency based on the linear complexity of Mamba. To further validate the robustness of the network to complex scenarios, the sixth column in Tab. 2 lists the experimental results of our network and different operators-based works on challenging ScanObjectNN (PB\_T50\_RS) dataset, where CloudMamba outperforms the state-of-the-art PointConT and PCM, which strongly proves its robustness.

### Point cloud part segmentation

Table 3 compares the experimental results of our network with different operators-based mainstream works on ShapeNet dataset. As shown in Tab. 3, our network achieves a higher Instance mIoU, and significantly improves the accuracy compared to the concurrent SSM-based works. It is worth noting that CloudMamba achieves the same Instance mIoU as the state-of-the-art Point Transformer with fewer FLOPs and Params, which fully validates our network is capable of adapting Mamba’s superior long-range modeling to point cloud analysis. Also, we observe CloudMamba requires only 1.234G FLOPs, significantly lower than the attention networks and other SSM networks, which demonstrates our network enables a lightweight architecture.

### Point cloud semantic segmentation

Table 4 compares the experimental results of our network and different operators-based mainstream works on S3DIS

Networks	Operators	FLOPs	Params	OA	
				Model.	Scan.
PointNet++ (2017b)	MLP	4.1	1.7	91.9	77.9
PointMLP (2022)	MLP	15.7	13.2	93.6	85.4
PointNext (2022)	MLP	1.6	1.4	93.2	87.7
DGCNN (2019)	CNN	-	-	92.9	78.1
3D-GCN (2022)	CNN	-	-	92.1	-
Point Transformer (2021)	Attention	18.4	9.6	<b>93.7</b>	-
Point-BERT (2022)	Attention	2.3	22.1	92.7	83.1
Point-MAE (2022)	Attention	2.4	22.1	93.2	85.2
OctFormer (2023)	Attention	0.6	3.4	92.7	-
IDPT (2023)	Attention	2.3	1.7	93.4	83.7
PointGST (2024a)	Attention	4.8	0.6	93.4	85.6
DAPT (2024)	Attention	5.0	1.1	93.1	85.4
LCM (2024)	Attention	1.3	2.7	93.6	87.8
PointTramba (2024b)	SSM & Attention	-	-	92.7	-
Mamba3D (2024)	SSM	3.9	16.9	93.4	87.6
PointMamba (2024b)	SSM	3.6	12.3	92.4	82.5
OctMamba (2024a)	SSM	1.3	3.1	92.7	-
PCM (2024)	SSM	45.0	34.2	92.6	88.1
SI-Mamba (2025)	SSM	3.6	12.3	92.7	87.3
CloudMamba	SSM	1.150	9.95	<b>93.7</b>	<b>88.3</b>

Table 2: Experimental results of our network and different operators-based mainstream works on ModelNet40 and ScanObjectNN datasets.

dataset. As shown in Tab. 4, fewer SSM-based networks are validated on difficult scene-level S3DIS dataset, while CloudMamba makes up for this deficiency, and further demonstrates our network’s exceptional long-range modeling capability and efficient linear complexity property by outperforming the state-of-the-art Point Transformer V3 with fewer FLOPs and params.

## Ablation studies

### Validity checking

In the proposed network, we design the sorting prompt, position embedding, and GS6 to further enhance the network performance. To demonstrate their validity, we compare the experimental results with and without these components, where the sorting prompt and position embedding are directly removed from the network when they are not used, and S6 is used as a replacement when GS6 is not used (*i.e.*, the grouping rate is set to 1 in GS6).

**Sorting prompt.** As shown in Group I in Tab. 5, the sorting prompt improves 0.46% OA, indicating that as the network continuously learns, the causal dependencies generated from different directions are confused, leading to incorrect shape understanding, and the sorting prompt, as a widget, can help the network clearly infer geometric structures from different dependencies with little effect on the FLOPs and Params.

**Position embedding.** Group II in Tab. 5 shows that the absence of the position embedding decreases 0.5% OA, which indicates that as the network deepens, higher-level features lose fine position information. Hence, it is necessary to facilitate geometric learning by continuously maintaining position information through the position embedding.

**GS6.** Group III in Tab. 5 shows GS6 improves 1.54% OA

Networks	Operator	FLOPs	Params	Ins.	mIoU
PointNet++ (2017b)	MLP	4.8	1.7	-	85.1
PointMLP (2022)	MLP	6.3	16.8	-	86.1
ReCon (2023)	MLP	-	-	-	86.4
DGCNN (2019)	CNN	-	-	-	85.2
3D-GCN (2022)	CNN	-	-	-	85.3
Point Transformer (2021)	Attention	36.7	19.4	-	<b>86.6</b>
PCT (2021)	Attention	4.4	2.9	-	86.4
Point-BERT (2022)	Attention	4.5	22.1	-	85.6
Point-MAE (2022)	Attention	4.8	22.1	-	86.1
MaskPoint (2022)	Attention	4.8	22.1	-	86.0
APES (2023)	Attention	-	-	-	85.8
IDPT (2023)	Attention	4.8	5.7	-	85.7
LCM (2024)	Attention	-	-	-	86.3
PointGST (2024a)	Attention	4.8	5.6	-	85.7
DAPT (2024)	Attention	5.0	5.7	-	85.5
PointTramba (2024b)	SSM & Attention	-	-	-	85.7
Mamba3D (2024)	SSM	11.8	23.0	-	85.6
PointMamba (2024b)	SSM	14.3	17.4	-	85.8
PCM (2024)	SSM	52.1	40.6	-	84.3
PMA (2025)	SSM	-	-	-	86.1
CloudMamba	SSM	1.234	16.57	-	<b>86.6</b>

Table 3: Experimental results of our network and different operators-based mainstream works on ShapeNet dataset.

Networks	Operator	FLOPs	Params	Ins.	mIoU
RandLA-Net (2022)	MLP	-	-	-	63.2
PointMeta (2023)	MLP	-	-	-	69.5
DGCNN (2019)	CNN	-	-	-	56.5
3D-GCN (2022)	CNN	-	-	-	58.6
Point Transformer (2021)	Attention	147.2	19.4	-	70.4
Point Transformer v2 (2022)	Attention	88.3	12.9	-	71.6
SuperpointTransformer (2023)	Attention	-	-	-	68.9
Point Transformer v3 (2024)	Attention	26.5	46.2	-	73.4
Grid Mamba (2025)	SSM	-	-	-	71.8
Pamba (2025)	SSM	-	-	-	73.5
PCM (2024)	SSM	72.1	40.6	-	63.4
CloudMamba	SSM	4.922	16.56	-	<b>73.6</b>

Table 4: Experimental results of our network and different operators-based mainstream works on S3DIS dataset.

while reducing 0.4M params, revealing the computational mode in S6 causes a certain degree of overfitting, and GS6 is able to alleviate this problem via the parameter sharing.

### Network property

**Causal dependency.** Our network forms three causal sequences, providing multiple perspectives for geometric perception. To explore the impact of these sequences, we perform separate experiments in combinations of the sequences from Z, Y, and X axes, as shown in Tab. 6, where more causal sequences involved are able to obtain a higher OA, which reveals more causal dependencies from multiple perspectives can help the network to learn stereoscopic geometry. Notably, no causal sorting of point sets (input directly) achieves a low OA, which reflects the causal nature of Mamba.

**Structure of the bidirectional Mamba.** Existing Mamba-based visual networks mostly follow the idea of Zhu *et al.*

	FLOPs (G)	Params (M)	OA (%)
I		Sorting prompt	
w/	1.150	9.95	<b>93.65</b>
w/o	1.150	9.95	93.19
II		Position embedding	
w/	1.150	9.95	<b>93.65</b>
w/o	1.141	9.70	93.15
III		GS6	
w/	1.150	9.95	<b>93.65</b>
w/o	1.150	10.35	92.11

Table 5: Experimental results of our network with and without the relevant components on ModelNet40 dataset.

Combination	FLOPs (G)	Params (M)	OA (%)
None	1.123	4.99	88.98
X	1.123	4.99	91.37
Y	1.123	4.99	90.96
Z	1.123	4.99	91.09
X, Y	1.136	7.47	92.38
X, Z	1.136	7.47	92.71
Y, Z	1.136	7.47	92.59
X, Y, Z	1.150	9.95	<b>93.65</b>

Table 6: Experimental results in combinations of the sequences from Z, Y, and X axes on ModelNet40 dataset, where None denotes point sets are not causally sorted.

Structure	FLOPs (G)	Params (M)	OA (%)
Parallel	1.150	9.95	92.69
Chained	1.150	9.95	<b>93.65</b>

Table 7: Experimental results with different structures of the bidirectional Mamba on ModelNet40 dataset.

(Zhu *et al.* 2024) to adapt Mamba’s unidirectional modeling to visual data, *i.e.*, the parallel bidirectional Mamba, but it results in insufficient high-level geometric perception compared to our chainedMamba. We compare the experimental results of this parallel structure with the chained structure adopted by our network. For a fair comparison, the experimental configurations are identical (including the number of the bidirectional Mamba, and the use of GS6) except for employing different structures of the bidirectional Mamba. Tab. 7 shows our chained structure obtains a higher OA, which means our structure is able to achieve more superior geometric perception and yield better expressivity.

## Conclusion

In this paper, we propose an SSM-based point cloud network termed CloudMamba, which overcomes the shortcomings of existing related works, including imperfect point cloud serialization, insufficient high-level geometric perception, and overfitting caused by the computational mode in S6, through the sequence expanding & merging, chainedMamba, and GS6. Extensive experiments demonstrate CloudMamba is able to obtain state-of-the-art results with linear complexity.

## Acknowledgments

This work is supported in part by the National Natural Science Foundation of China under Grant (62476126, 62272227).

## References

- Armeni, I.; Sener, O.; Zamir, A. R.; Jiang, H. L.; Brilakis, I.; Fischer, M.; and Savarese, S. 2016. 3D semantic parsing of large-scale indoor spaces. In *CVPR*, 1534–1543. Las Vegas, NV, USA.
- Bahri, A.; Yazdanpanah, M.; Noori, M.; Dastani, S.; Cheraghalikhani, M.; Osowiecki, D.; Hakim, G.; Beizae, F.; Ayed, I. B.; and Desrosiers, C. 2025. Spectral Informed Mamba for Robust Point Cloud Processing. In *CVPR*, 11799–11809. Nashville, TN, USA.
- Dao, T.; Fu, D. Y.; Ermon, S.; Rudra, A.; and Ré, C. 2022. FlashAttention: Fast and Memory-Efficient Exact Attention with IO-Awareness. In *NIPS*, 1–16. New Orleans, LA, USA.
- Dosovitskiy, A.; Beyer, L.; Kolesnikov, A.; Weissenborn, D.; Zhai, X. H.; Unterthiner, T.; Dehghani, M.; Minderer, M.; Heigold, G.; Gelly, S.; Uszkoreit, J.; and Houshly, N. 2021. An image is worth 16x16 words: Transformers for image recognition at scale. In *ICLR*, 1–22. Virtual Event, Austria.
- Fan, L.; Pang, Z. Q.; Zhang, T. Y.; Wang, Y. X.; Zhao, H.; Wang, F.; Wang, N. Y.; and Zhang, Z. X. 2022. Embracing single stride 3D object detector with sparse transformer. In *CVPR*, 8448–8458. New Orleans, LA, USA.
- Gu, A.; and Dao, T. 2023. Mamba: Linear-time sequence modeling with selective state spaces. arXiv:2312.00752.
- Gu, A.; Dao, T.; Ermon, S.; Rudra, A.; and Ré, C. 2020. Hippo: Recurrent memory with optimal polynomial projections. In *NIPS*, 1474–1487. Virtual Event.
- Gu, A.; Goel, K.; and Ré, C. 2022. Efficiently modeling long sequences with structured state spaces. In *ICLR*, 1–15. Virtual Event.
- Gu, A.; Johnson, I.; Goel, K.; Saab, K.; Dao, T.; Rudra, A.; and Ré, C. 2021. Combining recurrent, convolutional, and continuous-time models with linear state space layers. In *NIPS*, 572–585. Virtual Event.
- Guo, M. H.; Cai, J. X.; Liu, Z. N.; Mu, T. J.; Martin, R. R.; and Hu, S. M. 2021. PCT: Point cloud transformer. *Computational Visual Media*, 7(2): 187–199.
- Gupta, A.; Gu, A.; and Berant, J. 2022. Diagonal State Spaces are as Effective as Structured State Spaces. In *NIPS*, 1–12. New Orleans, LA, USA.
- Han, X.; Tang, Y.; Wang, Z. X.; and Li, X. Z. 2024. Mamba3D: Enhancing Local Features for 3D Point Cloud Analysis via State Space Model. In *ACM International Conference on Multimedia*, 1–10. Melbourne, Australia.
- Hilbert, D. 1935. Über die stetige abbildung einer linie auf ein flächenstück. In *Dritter Band: Analysis: Grundlagen der Mathematik· Physik Verschiedenes: Nebst Einer Lebensgeschichte*.
- Hu, Q. Y.; Yang, B.; Xie, L. H.; Rosa, S.; Guo, Y. L.; Wang, Z. H.; Trigoni, N.; and Markham, A. 2022. Learning Semantic Segmentation of Large-Scale Point Clouds With Random Sampling. *PAMI*, 44(11): 8338–8354.
- Li, Z. Y.; Ai, Y. B.; Lu, J. H.; Wang, C. X.; C., J.; Deng; Chang, H. Z.; Liang, Y. Z.; Yang, W. F.; Zhang, S. F.; and Zhang, T. Z. 2025. Pamba: Enhancing Global Interaction in Point Clouds via State Space Model. In *AAAI*, 5092–5100. Philadelphia, PA, USA.
- Liang, D. K.; Feng, T. R.; Zhou, X.; Zhang, Y. M.; Zou, Z. K.; and Bai, X. 2024a. Parameter-Efficient Fine-Tuning in Spectral Domain for Point Cloud Learning. arXiv:2410.08114.
- Liang, D. K.; Zhou, X.; Xu, W.; Zhu, X. K.; Zou, Z. K.; Ye, X. Q.; Tan, X.; and Bai, X. 2024b. PointMamba: A Simple State Space Model for Point Cloud Analysis. arXiv:2402.10739.
- Lin, H. J.; Zheng, X. W.; Li, L. J.; Chao, F.; Wang, S. S.; Wang, Y.; Tian, Y. H.; and Ji, R. R. 2023. Meta Architecture for Point Cloud Analysis. In *CVPR*, 17682–17691. Vancouver, BC, Canada.
- Lin, Z. H.; Huang, S. Y.; and Wang, Y. F. 2022. Learning of 3D Graph Convolution Networks for Point Cloud Analysis. *PAMI*, 44(8): 4212–4224.
- Liu, H. T.; Cai, M.; and Lee, Y. J. 2022. Masked discrimination for self-supervised learning on point clouds. In *ECCV*, 657–675. Tel Aviv, Israel.
- Liu, J. M.; Han, J. R.; Liu, L. H.; Aviles-Rivero, A. I.; Jiang, C. K.; Liu, Z.; and Wang, H. S. 2025. Mamba4D: Efficient 4D Point Cloud Video Understanding with Disentangled Spatial-Temporal State Space Models. In *CVPR*, 17626–17636. Nashville, TN, USA.
- Liu, J. M.; Yu, R. J.; Wang, Y.; Zheng, Y.; Deng, T. C.; Ye, W. C.; and Wang, H. S. 2024a. Point Mamba: A Novel Point Cloud Backbone Based on State Space Model with Octree-Based Ordering Strategy. arXiv:2403.06467.
- Liu, Y.; Tian, Y. J.; Zhao, Y. Z.; Yu, H. T.; Xie, L. X.; Wang, Y. W.; Ye, Q. X.; and Liu, Y. F. 2024b. VMamba: Visual State Space Model. arXiv:2401.10166.
- Liu, Z. J.; Yang, X. Y.; Tang, H. T.; Yang, S.; and Han, S. 2023. FlatFormer: Flattened Window Attention for Efficient Point Cloud Transformer. In *CVPR*, 1200–1211. Vancouver, BC, Canada.
- Ma, J.; Li, F. F.; and Wang, B. 2024. U-Mamba: Enhancing Long-range Dependency for Biomedical Image Segmentation. arXiv:2401.04722.
- Ma, X.; Qin, C.; You, H. X.; Ran, H. X.; and Fu, Y. 2022. Rethinking Network Design and Local Geometry in Point Cloud: A Simple Residual MLP Framework. In *ICLR*, 1–14. Virtual Event.
- Martin, E.; and Cundy, C. 2018. Parallelizing linear recurrent neural nets over sequence length. In *ICLR*, 1–9. Vancouver, BC, Canada.
- Mehta, H.; Gupta, A.; Cutkosky, A.; and Neyshabur, B. 2022. Long range language modeling via gated state spaces. arXiv:2206.13947.
- Nie, D.; Lan, R.; Wang, L.; and Ren, X. F. 2022. Pyramid Architecture for Multi-Scale Processing in Point Cloud Segmentation. In *CVPR*, 17263–17273. New Orleans, LA, USA.

- Pang, Y. T.; Wang, W. X.; Tay, F. E. H.; Liu, W.; Tian, Y. H.; and Yuan, L. 2022. Masked Autoencoders for Point Cloud Self-supervised Learning. In *ECCV*, 604–621. Tel Aviv, ISRAEL.
- Park, C.; Jeong, Y.; Cho, M. S.; and Park, J. 2022. Fast point transformer. In *CVPR*, 16928–16937. New Orleans, LA, USA.
- Qi, C. R.; Su, H.; Mo, K. C.; and Guibas, L. J. 2017a. Pointnet: Deep learning on point sets for 3d classification and segmentation. In *CVPR*, 77–85. Honolulu, HI, USA.
- Qi, C. R.; Yi, L.; Su, H.; and Guibas, L. J. 2017b. Pointnet++: Deep hierarchical feature learning on point sets in a metric space. In *NIPS*, 5099–5108. Long Beach, CA, USA.
- Qi, Z. K.; Dong, R. P.; Fan, G. F.; Ge, Z.; Zhang, X. Y.; Ma, K. S.; and Yi, L. 2023. Contrast with Reconstruct: Contrastive 3D Representation Learning Guided by Generative Pretraining. In *ICML*, 28223–28243. Honolulu, HI, USA.
- Qian, G. C.; Li, Y. C.; Peng, H. W.; Mai, J. J.; Hammoud, H. A. A. K.; Elhoseiny, M.; and Ghanem, B. 2022. PointNeXt: Revisiting PointNet++ with Improved Training and Scaling Strategies. In *NIPS*, 1–13. New Orleans, LA, USA.
- Robert, D.; Raguet, H.; and Landrieu, L. 2023. Efficient 3d semantic segmentation with superpoint transformer. In *ICCV*, 1–10. Paris, France.
- Ronneberger, O.; Fischer, P.; and Brox, T. 2015. U-Net: Convolutional Networks for Biomedical Image Segmentation. In *International Conference on Medical Image Computing and Computer-Assisted Intervention*, 234–241. Munich, Germany.
- Ruan, J. C.; and Xiang, S. C. 2024. VM-UNet: Vision Mamba UNet for Medical Image Segmentation. arXiv:2402.02491.
- Smith, J. T. H.; Warrington, A.; and Linderman, S. W. 2022. Simplified state space layers for sequence modeling. arXiv:2208.04933.
- Uy, M. A.; Pham, Q. H.; Hua, B. S.; Nguyen, D. T.; and Yeung, S. K. 2019. Revisiting Point Cloud Classification: A New Benchmark Dataset and Classification Model on Real-World Data. In *ICCV*, 1588–1597. Seoul, South Korea.
- Vaswani, A.; Shazeer, N.; Parmar, N.; Uszkoreit, J.; Jones, L.; Gomez, A. N.; Kaiser, L.; and Polosukhin, I. 2017. Attention is all you need. In *NIPS*, 5998–6008. Long Beach, CA, USA.
- Wang, C.; Tsepa, O.; Ma, J.; and Wang, B. 2024a. Graph-Mamba: Towards Long-Range Graph Sequence Modeling with Selective State Spaces. arXiv:2402.00789.
- Wang, P. S. 2023. OctFormer: Octree-based Transformers for 3D Point Clouds. *TOG*, 42(4): 155.
- Wang, Y.; Sun, Y. B.; Liu, Z. W.; Sarma, S. E.; Bronstein, M. M.; and Solomon, J. M. 2019. Dynamic Graph CNN for Learning on Point Clouds. *TOG*, 38(5): 146.
- Wang, Z. C.; Chen, Z. H.; Wu, Y. M.; Zhao, Z.; Zhou, L. P.; and Xu, D. 2024b. PoinTramba: A Hybrid Transformer-Mamba Framework for Point Cloud Analysis. arXiv:2405.15463.
- Wu, C. Z.; Zheng, J. W.; Pfaffner, J.; and Beyerer, J. 2023. Attention-Based Point Cloud Edge Sampling. In *CVPR*, 5333–5343. Vancouver, BC, Canada.
- Wu, X. Y.; Jiang, L.; Wang, P. S.; Liu, Z. J.; Liu, X. H.; Qiao, Y.; Ouyang, W. L.; He, T.; and Zhao, H. S. 2024. Point Transformer V3: Simpler, Faster, Stronger. In *CVPR*, 1–15. Seattle, WA, USA.
- Wu, X. Y.; Lao, Y. X.; Jiang, L.; Liu, X. H.; and Zhao, H. S. 2022. Point transformer V2: Grouped vector attention and partition-based pooling. In *NIPS*, 1–13. New Orleans, LA, USA.
- Wu, Z. R.; Song, S. R.; Khosla, A.; Yu, F.; Zhang, L. G.; Tang, X. O.; and Xiao, J. X. 2015. 3d shapenets: A deep representation for volumetric shapes. In *CVPR*, 1912–1920. Boston, MA, USA.
- Yang, Y. L.; Xun, T. Z.; Hao, K. R.; Wei, B.; and Tang, X. S. 2025. Grid Mamba: Grid State Space Model for Large-Scale Point Cloud Analysis. *Neurocomputing*, 636: 129985.
- Yi, L.; Kim, V. G.; Ceylan, D.; Shen, I. C.; Yan, M. Y.; Su, H.; Lu, C.; Huang, Q. X.; Sheffer, A.; and Guibas, L. 2016. A scalable active framework for region annotation in 3d shape collections. *TOG*, 35(6): 210.
- Yu, X. M.; Tang, L. L.; Rao, Y. M.; Huang, T. J.; Zhou, J.; and Lu, J. W. 2022. Point-BERT: Pre-training 3D Point Cloud Transformers with Masked Point Modeling. In *CVPR*, 19291–19300. New Orleans, LA, USA.
- Zha, Y. H.; Li, N. Q.; Wang, Y. Z.; Dai, T.; Guo, H.; Chen, B.; Wang, Z.; Ouyang, Z. H.; and Xia, S. T. 2024. LCM: Locally Constrained Compact Point Cloud Model for Masked Point Modeling. In *NIPS*, 1–14. Vancouver, BC, Canada.
- Zha, Y. H.; Wang, J. P.; Dai, T.; Chen, B.; Wang, Z.; and Xia, S. T. 2023. Instance-aware Dynamic Prompt Tuning for Pre-trained Point Cloud Models. In *ICCV*, 1–10. Paris, France.
- Zha, Y. H.; Wang, Y. Z.; Guo, H.; Wang, J. P.; Dai, T.; Chen, B.; Ouyang, Z. H.; Xue, Y. R.; Chen, K.; and Xia, S. T. 2025. PMA: Towards Parameter-Efficient Point Cloud Understanding via Point Mamba Adapter. In *CVPR*, 16976–16986. Nashville, TN, USA.
- Zhang, T.; Li, X. T.; Yuan, H. B.; Ji, S. P.; and Yan, S. C. 2024. Point Cloud Mamba: Point Cloud Learning via State Space Model. arXiv:2403.00762.
- Zhao, H. S.; Jiang, L.; Jia, J. Y.; Torr, P.; and Koltun, V. 2021. Point transformer. In *ICCV*, 16239–16248. Montreal, BC, Canada.
- Zhou, X.; Liang, D. K.; Xu, W.; Zhu, X. K.; Xu, Y. H.; Zou, Z. K.; and Bai, X. 2024. Dynamic Adapter Meets Prompt Tuning: Parameter-Efficient Transfer Learning for Point Cloud Analysis. In *CVPR*, 14707–14717. Seattle, WA, USA.
- Zhu, L. H.; Liao, B. C.; Zhang, Q.; Wang, X. L.; Liu, W. Y.; and Wang, X. G. 2024. Vision Mamba: Efficient Visual Representation Learning with Bidirectional State Space Model. In *ICML*, 1–10. Vienna, Austria.

# CloudMamba: Grouped Selective State Spaces for Point Cloud Analysis

## Supplementary Material

### Appendix A Discretization of continuous SSMs

In this section, we deduce in detail the process of discretizing continuous SSMs by the zero-order holding method.

The state equation of continuous SSMs is as follows

$$h'(t) = \mathbf{A}h(t) + \mathbf{B}x(t). \quad (8)$$

Simultaneously multiplied by  $e^{-\mathbf{A}t}$ :

$$\begin{aligned} e^{-\mathbf{A}t}h'(t) &= e^{-\mathbf{A}t}\mathbf{A}h(t) + e^{-\mathbf{A}t}\mathbf{B}x(t), \\ e^{-\mathbf{A}t}h'(t) - e^{-\mathbf{A}t}\mathbf{A}h(t) &= e^{-\mathbf{A}t}\mathbf{B}x(t), \\ \frac{d[e^{-\mathbf{A}t}h(t)]}{dt} &= e^{-\mathbf{A}t}\mathbf{B}x(t). \end{aligned} \quad (9)$$

Followed by simultaneous integrals:

$$\begin{aligned} \int_{t_{(k-1)}}^{t_k} d[e^{-\mathbf{A}t}h(t)] &= \int_{t_{(k-1)}}^{t_k} e^{-\mathbf{A}t}\mathbf{B}x(t) dt, \\ e^{-\mathbf{A}t_k}h(t_k) - e^{-\mathbf{A}t_{(k-1)}}h(t_{(k-1)}) &= \int_{t_{(k-1)}}^{t_k} e^{-\mathbf{A}\tau}\mathbf{B}x(\tau) d\tau, \\ e^{-\mathbf{A}t_k}h(t_k) &= e^{-\mathbf{A}t_{(k-1)}}h(t_{(k-1)}) + \int_{t_{(k-1)}}^{t_k} e^{-\mathbf{A}\tau}\mathbf{B}x(\tau) d\tau, \\ h(t_k) &= e^{\mathbf{A}(t_k - t_{(k-1)})}h(t_{(k-1)}) + \int_{t_{(k-1)}}^{t_k} e^{\mathbf{A}(t_k - \tau)}\mathbf{B}x(\tau) d\tau, \\ h(t_k) &= e^{\Delta\mathbf{A}}h(t_{(k-1)}) + \int_{t_{(k-1)}}^{t_k} e^{\mathbf{A}(t_k - \tau)}\mathbf{B}x(\tau) d\tau. \end{aligned} \quad (10)$$

Let  $\nu = t_k - \tau$ , then  $d\nu = -d\tau$ . Since the zero-order holding makes  $x(t)$  a constant  $x_k$ , Eq. 10 is simplified to:

$$\begin{aligned} h(t_k) &= e^{\Delta\mathbf{A}}h(t_{(k-1)}) + \int_{t_{(k-1)}}^{t_k} e^{\mathbf{A}(t_k - \tau)}\mathbf{B}x(\tau) d\tau \\ &= e^{\Delta\mathbf{A}}h(t_{(k-1)}) - \int_{\Delta}^0 e^{\mathbf{A}\nu}d\nu\mathbf{B}x_k \\ &= e^{\Delta\mathbf{A}}h(t_{(k-1)}) + \int_0^{\Delta} e^{\mathbf{A}\nu}d\nu\mathbf{B}x_k \\ &= e^{\Delta\mathbf{A}}h(t_{(k-1)}) + \frac{(e^{\Delta\mathbf{A}} - \mathbf{I})\Delta}{\Delta\mathbf{A}}\mathbf{B}x_k, \end{aligned} \quad (11)$$

By writing the above in a discrete form:

$$\begin{aligned} h_k &= e^{\Delta\mathbf{A}}h_{k-1} + (\Delta\mathbf{A})^{-1}(e^{\Delta\mathbf{A}} - \mathbf{I})(\Delta\mathbf{B})x_k, \\ h_k &= \bar{\mathbf{A}}h_{k-1} + \bar{\mathbf{B}}x_k, \end{aligned} \quad (12)$$

where  $\bar{\mathbf{A}} = e^{\Delta\mathbf{A}}$  and  $\bar{\mathbf{B}} = (\Delta\mathbf{A})^{-1}(e^{\Delta\mathbf{A}} - \mathbf{I})(\Delta\mathbf{B})$ .

### Appendix B Relationship between S6 (Mamba) and the self-attention

For an input sequence  $\mathbf{x} = \{x_1, x_2, \dots, x_L\} \in \mathbb{R}^{L \times D}$ , S6 regards  $\Delta$ ,  $\mathbf{B}$ , and  $\mathbf{C}$  in Eq. 3 as the functions of  $\mathbf{x}$ . Therefore,  $\Delta_t$ ,  $\mathbf{B}_t$ , and  $\mathbf{C}_t$  in the  $t$ -th time step is computed as follows

$$\begin{aligned} \Delta_t &= \log\left(1 + e^{\text{Linear}^\Delta(x_t)}\right), \\ \mathbf{B}_t &= \text{Linear}^{\mathbf{B}}(x_t), \\ \mathbf{C}_t &= \text{Linear}^{\mathbf{C}}(x_t), \end{aligned} \quad (13)$$

where  $\text{Linear}^\Delta$  denotes a linear projection used for  $\Delta$ . Taking Eq. 13 into Eq. 3 yields  $\Delta_t$ ,  $\bar{\mathbf{A}}_t$ ,  $\bar{\mathbf{B}}_t$ , and  $\mathbf{C}_t$ . Next, we unfold Eq. 2, then the output  $\mathbf{y} = \{y_1, y_2, \dots, y_L\} \in \mathbb{R}^{L \times D}$  is computed as follows

$$\begin{aligned} h_t &= \sum_{i=1}^t \left( \prod_{j=i+1}^t \bar{\mathbf{A}}_j \right) \bar{\mathbf{B}}_i x_i, \\ y_t &= \mathbf{C}_t h_t. \end{aligned} \quad (14)$$

$h_t$  in Eq. 14 can be expressed in a matrix form:

$$\begin{bmatrix} h_1 \\ h_2 \\ \vdots \\ h_t \end{bmatrix} = \begin{bmatrix} \bar{\mathbf{B}}_1 & 0 & \cdots & 0 \\ \bar{\mathbf{A}}_2 \bar{\mathbf{B}}_1 & \bar{\mathbf{B}}_2 & \cdots & 0 \\ \vdots & \vdots & \ddots & 0 \\ \prod_{j=2}^t \bar{\mathbf{A}}_j \bar{\mathbf{B}}_1 & \prod_{j=3}^t \bar{\mathbf{A}}_j \bar{\mathbf{B}}_2 & \cdots & \bar{\mathbf{B}}_t \end{bmatrix} \begin{bmatrix} x_1 \\ x_2 \\ \vdots \\ x_t \end{bmatrix}. \quad (15)$$

As a result, the transformation matrix  $\mathbf{W}$  from  $\mathbf{x}$  to  $\mathbf{y}$  can be expressed as

$$\begin{aligned} \mathbf{W}_{i,j} &= \mathbf{C}_i \left( \prod_{s=j+1}^i \bar{\mathbf{A}}_s \right) \bar{\mathbf{B}}_j \\ &= \mathbf{C}_i \left( \prod_{s=j+1}^i e^{\Delta_s \mathbf{A}} \right) \bar{\mathbf{B}}_j \\ &= \mathbf{C}_i e^{\left( \sum_{s=j+1}^i \Delta_s \mathbf{A} \right)} \bar{\mathbf{B}}_j \\ &= \mathbf{C}_i e^{\left( \sum_{s=j+1}^i \log\left(1 + e^{\text{Linear}^\Delta(x_s)}\right) \mathbf{A} \right)} \bar{\mathbf{B}}_j. \end{aligned} \quad (16)$$

Let  $\mathbf{Q}_i = \mathbf{C}_i$ ,  $\mathbf{K}_j = (\bar{\mathbf{B}}_j)^T$ , and  $\mathbf{H}_{i,j} = e^{\left( \sum_{s=j+1}^i \log\left(1 + e^{\text{Linear}^\Delta(x_s)}\right) \mathbf{A} \right)}$ , then Eq. 16 can be abbreviated as

$$\mathbf{W}_{i,j} = \mathbf{Q}_i \mathbf{H}_{i,j} \mathbf{K}_j^T. \quad (17)$$

Eq. 17 indicates S6 captures the effects of  $x_i$  and  $x_j$  by  $\mathbf{Q}_i$  and  $\mathbf{K}_j^T$ , respectively, and that  $\mathbf{H}_{i,j}$  contains causal information from  $x_i$  to  $x_j$ . Note that  $\mathbf{W}_{i,j}$  is similar to the attention mechanism with a mask  $\mathbf{M}$  (a lower triangular matrix with elements set to 1), *i.e.*, the causal self-attention, which reveals that S6 is a special causal self-attention modulated by  $\mathbf{H}_{i,j}$ . Moreover, it is known from Eq. 16 that the causal information contained in  $\mathbf{H}_{i,j}$  is directly affected by  $\mathbf{A}$ , which explains the importance of designing the Hippo algorithm by Gu *et al.* (Gu *et al.* 2020) to obtain more accurate causal information.

## Appendix C Datasets and evaluation metrics

ModelNet40 is a well-segmented synthetic recognition dataset containing 12,311 samples with 40 categories, of which 9,843 samples are used for training and 2,468 samples used for testing. Following the data preprocessing of Qi *et al.* (Qi et al. 2017a), 1024 points (normalized to a unit sphere) and their corresponding normal vectors are uniformly sampled. As per most relevant studies in the literature, we adopt the overall accuracy (OA) as an evaluation metric.

ScanObjectNN is a challenging recognition dataset from the real world. This dataset introduces several variants through the perturbation. We conduct experiments on the most difficult variant, PB.T50.RS, to validate the robustness of CloudMamba, where the suffixes T50, R, and S denote randomly shifting the bounding box by 50% along each axis, rotation, and scaling, respectively. This variant contains about 15,000 valid samples with 15 categories, where 80% of the samples are used for training and 20% of the samples are used for testing. We use the same data preprocessing and evaluation metric as on ModelNet40 dataset.

ShapeNet is a large-scale part segmentation dataset containing 16,878 samples with 50 parts from 16 categories, of which 14,005 samples are used for training and 2,874 samples are used for testing. We adopt the same data preprocessing as on ModelNet40 dataset and use the Instance mIoU (Ins. mIoU) as an evaluation metric according to general practice in the community.

S3DIS is a scene-level semantic segmentation dataset that includes 3D scanned points from 271 rooms in 6 regions, with 13 semantic label categories. We follow the data preprocessing procedure of Qi *et al.* (Qi et al. 2017a) and take point coordinates, RGB, and normalized position as inputs. As per most relevant studies in the literature, region 5 is used as test set and the other regions are used for training, and the mean IoU (mIoU) is used as an evaluation metric.

## Appendix D Effect of the grouping rate

Group III in Tab. 5 demonstrates that GS6 can alleviate a certain degree of overfitting caused by S6 through the parameter sharing, where the grouping rate parameter determines how many dimensions share the same set of parameters in GS6. Therefore, we continuously increase the grouping rate to explore its effect on the network. Tab. 8 reveals that the overfitting of S6 is gradually alleviated as the grouping rate increases, but it leads to underfitting when it is overlarge. The grouping rate is a hyperparameter similar to the number of heads in the multi-head self-attention. Hence, it is important to set an appropriate grouping rate for the performance of GS6 based on the model scale, and when deploying the model to another data, we recommend setting the grouping rate starting from 3 and gradually increasing it until performance degradation is observed.

## Appendix E Comparison with other SSM-based networks

To intuitively demonstrate that our CloudMamba is able to achieve state-of-the-art results with less computational resources in contemporaneous SSM-based networks, we vi-

Grouping rate	FLOPs (G)	Params (M)	OA (%)
1	1.150	10.35	93.11
2	1.150	10.05	93.35
3 <sup>††</sup>	1.150	9.95	<b>93.65</b>
6	1.150	9.85	92.75
9	1.150	9.82	92.14

Table 8: Experimental results of our network with different grouping rates on ModelNet40 dataset. <sup>††</sup> indicates a baseline parameter.

sualize the accuracy of each SSM network on ModelNet40 dataset, as well as the FLOPs and Params. As shown in Fig. 5, our network achieve state-of-the-art accuracy with less FLOPs and Params among SSM networks.

## Appendix F Point cloud serialization

It is crucial to construct structural dependencies in a sequence via point cloud serialization for Mamba’s causal inference. At present, space-filling curves are one of main serialization strategies, among which the Hilbert curve and its variant Trans-Hilbert are commonly used methods in the community. Hence, we apply both to the causal dependency construction of our network to replace the sequence expanding module. Since the grid size is a core parameter of space-filling curves for restricting each point to the corresponding grid, we set different grid sizes for the Hilbert curve. The comparison in Tab. 1 demonstrates that space-filling curves are highly sensitive to the grid size, while our proposed sequence expanding is simple yet effective.

## Appendix G Linear complexity

Mamba achieves efficient computation by the parallel scanning algorithm with linear complexity. To validate our network inherits this property, we continuously increase the number of input points to observe changes on the FLOPs, while adding Point Transformer (Zhao et al. 2021) and PCM (Zhang et al. 2024) as a contrast, as shown in Fig. 6, which demonstrates the feasibility of our network for long sequence modeling in terms of computational overheads.

## Appendix H Limitations

While our network shows its potential in 3D vision, there is still room for further improvement, especially by self-supervised pre-training. The previous works (Yu et al. 2022; Pang et al. 2022; Liu, Cai, and Lee 2022) have validated it is effective to perform self-supervised pre-training on large-scale point cloud datasets for improving the accuracy. However, the compatibility of existing pre-training methods on SSM-based architectures, as well as pre-training techniques tailored for this type of networks remain unexplored.

In addition, this paper constructs structural dependencies by sorting points along each axis, which destroys geometric structures to a certain extent, and although this problem can be mitigated by merging higher-order interaction features causally inferred from each axis, it may still render the network to struggle to learn geometric structures.

Networks	Airplane #341	Bag #14	Cap #11	Car #158	Chair #704	Earphone #14	Guitar #159	Knife #80	Lamp #286	Laptop #83	Motorbike #51	Mug #38	Pistol #44	Rocket #12	Skateboard #31	Table #848
PointNet++	82.4	79.0	87.7	77.3	90.8	71.8	91.0	85.9	83.7	95.3	71.6	94.1	81.3	58.7	76.4	82.6
PointNet	83.4	78.7	82.5	74.9	89.6	73.0	91.5	85.9	80.8	95.3	65.2	93.0	81.2	57.9	72.8	80.6
PointMLP	83.5	83.4	87.5	80.5	90.3	78.2	<b>92.2</b>	<b>88.1</b>	82.6	96.2	<b>77.5</b>	95.8	<b>85.4</b>	64.6	<b>83.3</b>	84.3
3D-GCN	82.8	<b>86.1</b>	84.8	79.2	91.1	74.9	91.6	87.4	83.6	95.8	69.3	94.9	82.4	61.1	75.6	82.2
DGCNN	84.0	83.4	86.7	77.8	90.6	74.7	91.2	87.5	82.8	95.7	66.3	94.9	81.1	63.5	74.5	82.6
SpiderCNN	83.5	81.0	87.2	77.5	90.7	76.8	91.1	87.3	83.3	95.8	70.2	93.5	82.7	59.7	75.8	82.8
PointASNL	84.1	84.7	87.9	79.7	<b>92.2</b>	73.7	91.0	87.2	84.2	95.8	74.4	95.2	81.0	63.0	76.3	83.2
PCT	85.0	82.4	89.0	<b>81.2</b>	91.9	71.5	91.3	<b>88.1</b>	<b>86.3</b>	95.8	64.6	95.8	83.6	62.2	77.6	83.7
ACT	<b>85.2</b>	85.2	88.8	<b>81.2</b>	91.3	79.4	<b>92.2</b>	87.9	85.8	96.0	75.5	95.5	85.2	<b>66.6</b>	77.7	81.5
Point-BERT	84.3	84.8	88.0	79.8	91.0	<b>81.7</b>	91.6	87.9	85.2	95.6	75.6	94.7	84.3	63.4	76.3	81.5
Point-MAE	84.3	85.0	88.3	80.5	91.3	78.5	92.1	87.4	86.1	96.1	75.2	94.6	84.7	63.5	77.1	82.4
MaskPoint	84.2	85.6	88.1	80.3	91.2	79.5	91.9	87.8	86.2	95.3	76.9	95.0	85.3	64.4	76.9	81.8
CloudMamba	84.5	83.3	<b>91.7</b>	79.2	<b>92.2</b>	72.9	91.7	87.9	84.8	<b>96.5</b>	59.6	<b>96.2</b>	82.2	62.7	74.2	<b>84.5</b>

Table 9: mIoU on each category in ShapeNet dataset by CloudMamba and comparison networks.

Airplane #100	Bathtub #50	Bed #100	Bench #20	Bookshelf #100	Bottle #100	Bowl #20	Car #100	Chair #100	Cone #20
1.00	0.94	1.00	0.80	0.97	0.97	0.90	0.99	0.97	1.00
Cup #20	Curtain #20	Desk #86	Door #20	Dresser #86	Flower_pot #20	Glass_box #100	Guitar #100	Keyboard #20	Lamp #20
0.70	0.90	0.87	0.90	0.81	0.55	0.96	0.99	1.00	0.95
Laptop #20	Mantel #100	Monitor #100	Night_stand #86	Person #20	Piano #100	Plant #100	Radio #20	Range_hood #100	Sink #20
1.00	0.96	0.99	0.92	1.00	0.91	0.89	0.90	0.92	0.90
Sofa #100	Stairs #20	Stool #20	Table #100	Tent #20	Toilet #100	Tv_stand #100	Vase #100	Wardrobe #20	Xbox #20
0.98	0.80	0.85	1.00	0.95	0.99	0.91	0.87	0.75	0.80

Table 10: Accuracy of our network on each category in ModelNet40 dataset.

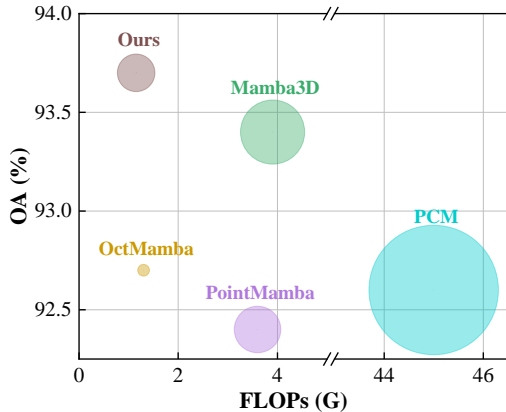


Figure 5: Comparison of SSM-based networks on ModelNet40 dataset, where a larger circle means more parameters.

Hence, it is a future endeavor to explore these aspects to make SSM-based works fully outperform attention networks in terms of accuracy in various point cloud tasks.

### Appendix I Detailed experimental results

For ShapeNet dataset, we list the mIoU of CloudMamba and the comparative networks on each category in Tab. 9 to clearly show the performance of our network on each cat-

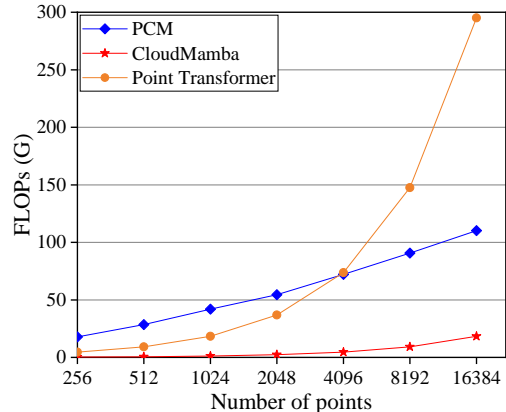


Figure 6: Changes of different networks on the FLOPs as the number of points increases.

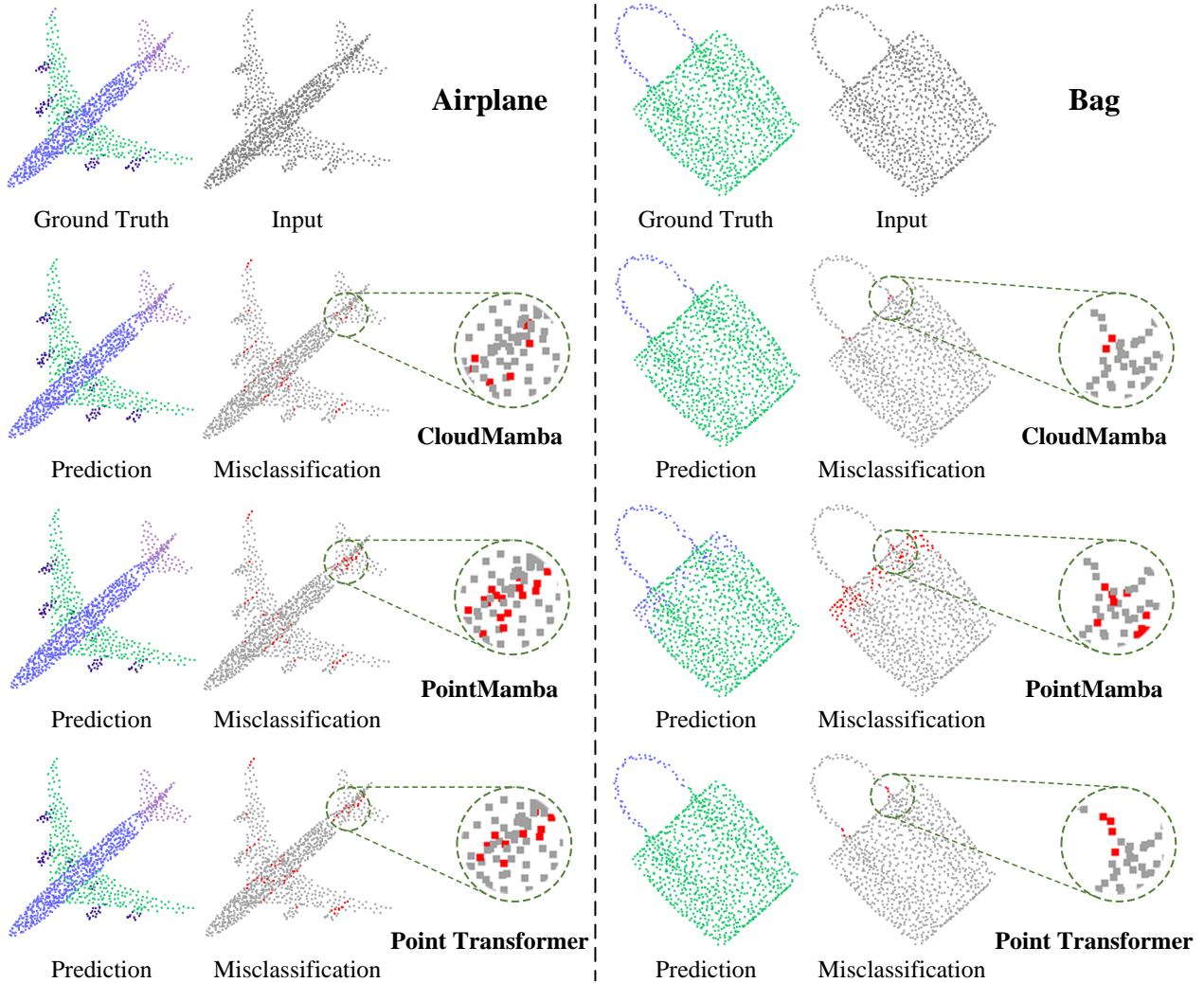
egory. By comparison, we find that CloudMamba achieves the highest mIoU on up to five categories in ShapeNet dataset, and this best result in comparison to the other networks demonstrates our network’s ability to effectively leverage and extend Mamba’s superior long-range modeling capability, showcasing the potential of SSM in point cloud analysis. In addition, Fig. 7 shows the qualitative results of CloudMamba, PointMamba (Liang et al. 2024b), and Point

Bag #100	Bin #176	Box #108	Cabinet #360	Chair #340	Desk #165	Display #174	Door #200
0.78	0.85	0.67	0.90	0.91	0.89	0.91	0.93
Shelf #222	Table #233	Bed #115	Pillow #124	Sink #115	Sofa #235	Toilet #75	
0.90	0.86	0.86	0.87	0.91	0.92	0.88	

Table 11: Accuracy of our network on each category in ScanObjectNN dataset.

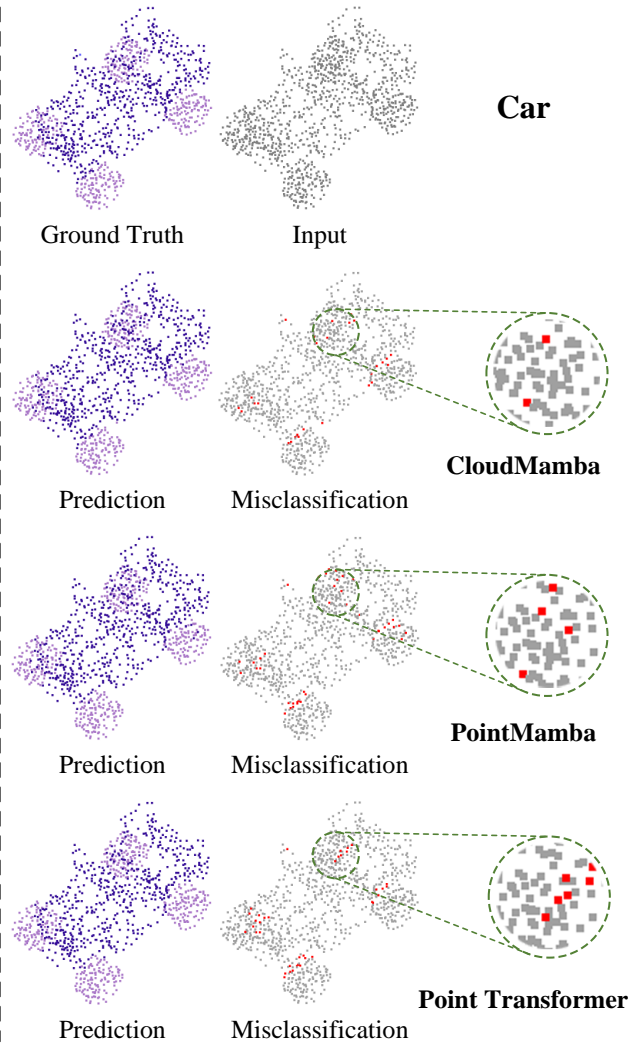
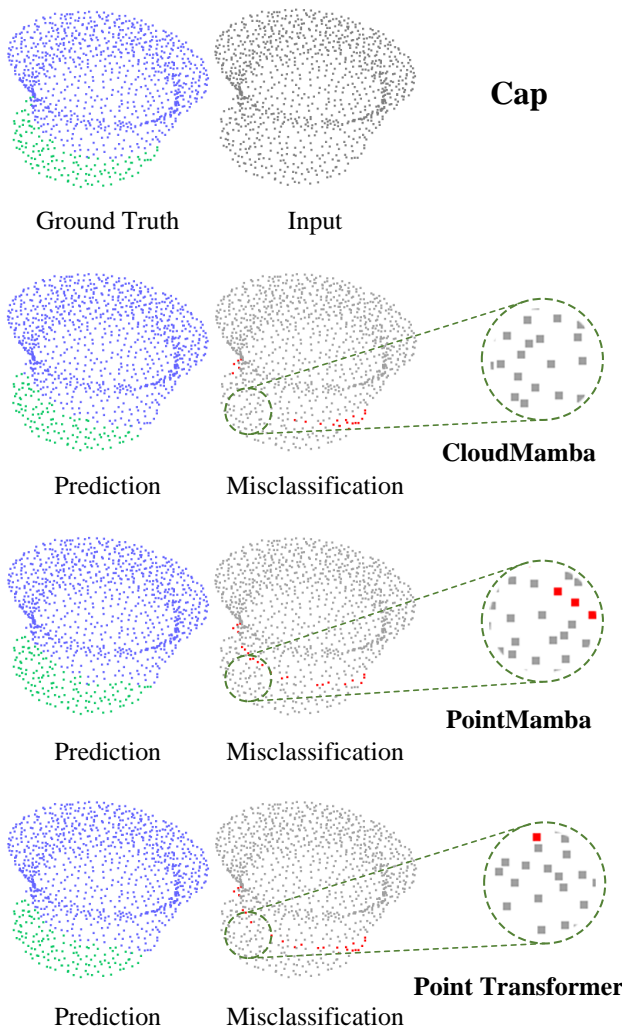
Ceiling	Floor	Wall	Beam	Column	Window	Door
96.1	98.4	87.8	0.0	44.5	65.1	75.7
Table	Chair	Sofa	Bookcase	Board	Clutter	
89.4	88.4	84.2	79.4	79.8	67.4	

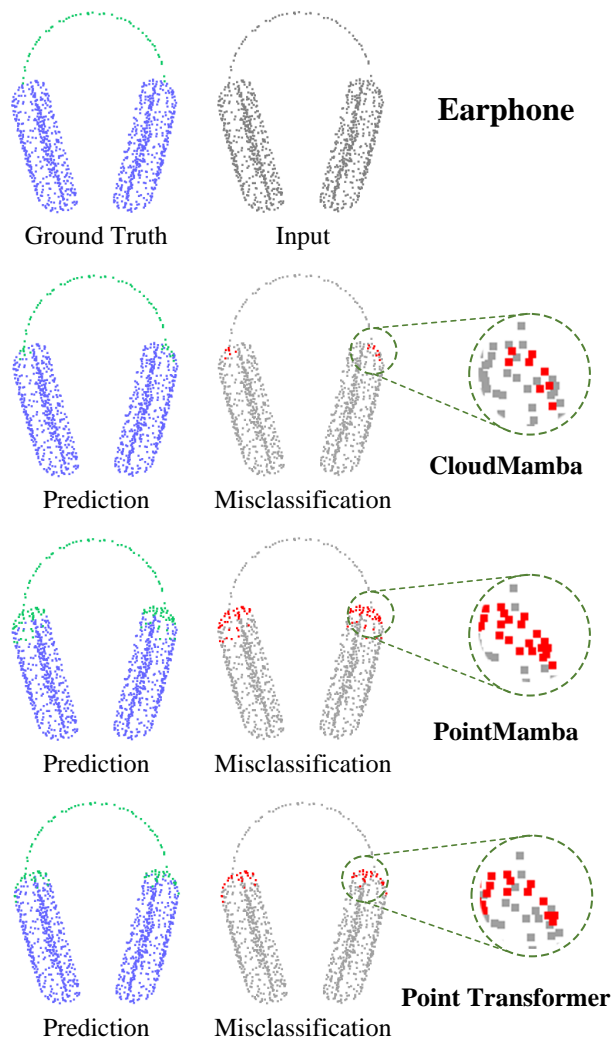
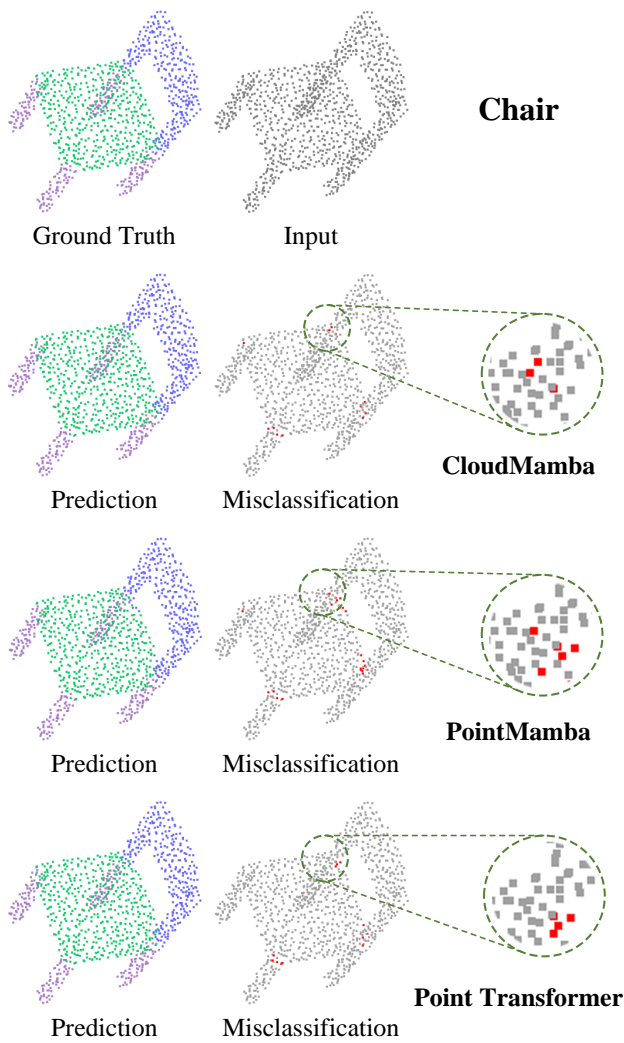
Table 12: IoU of our network on each category in S3DIS dataset.

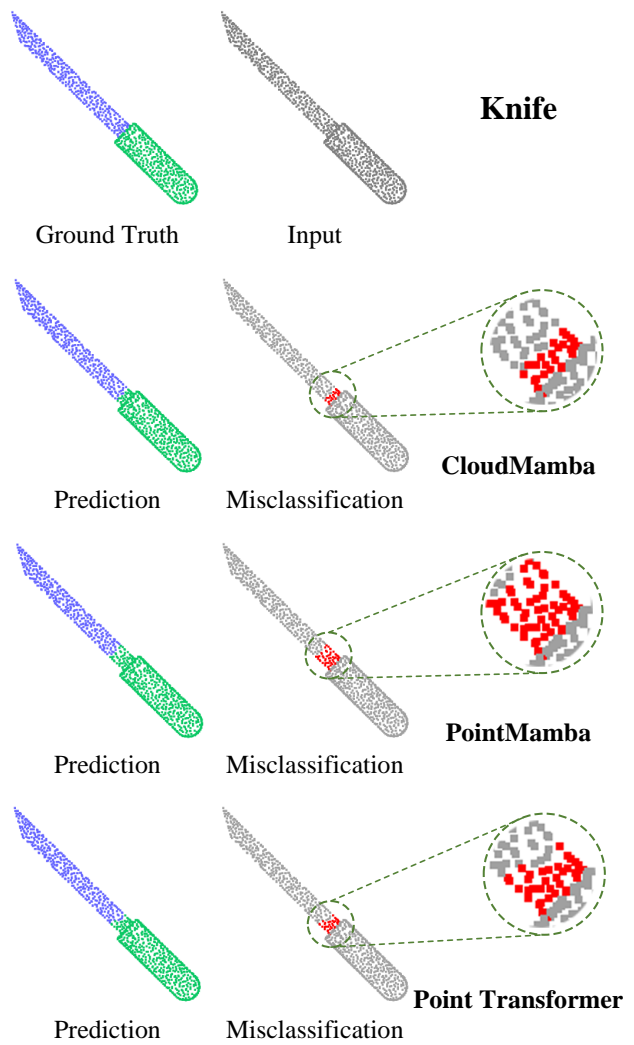
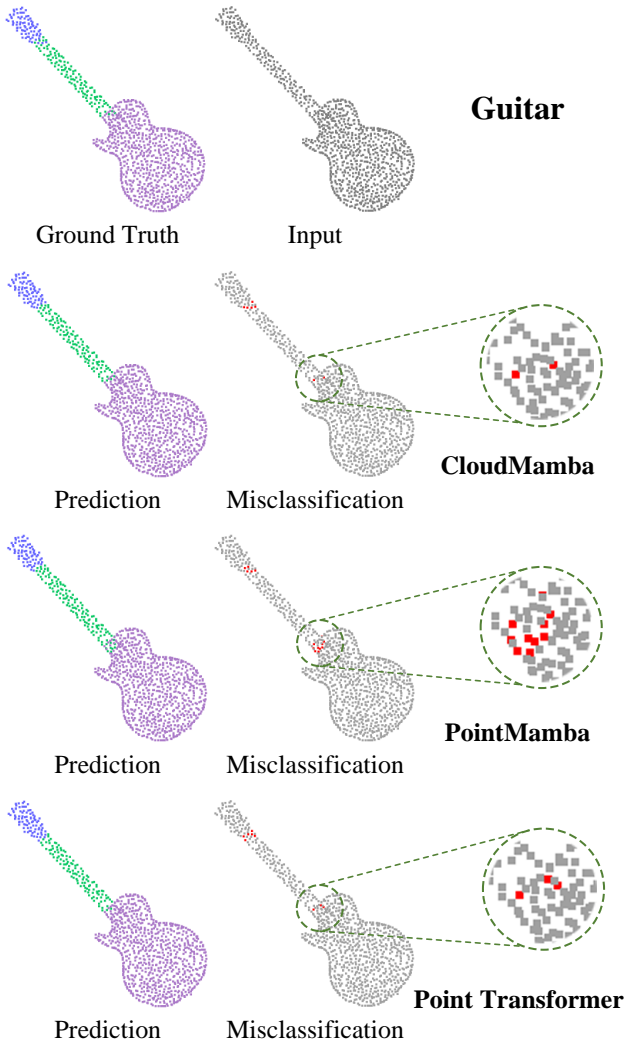


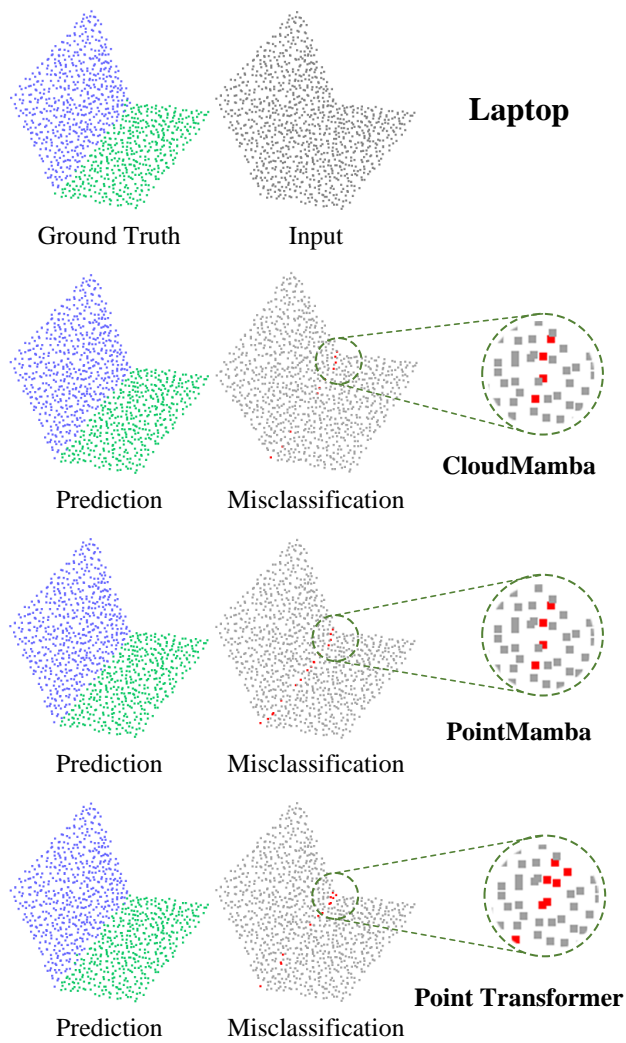
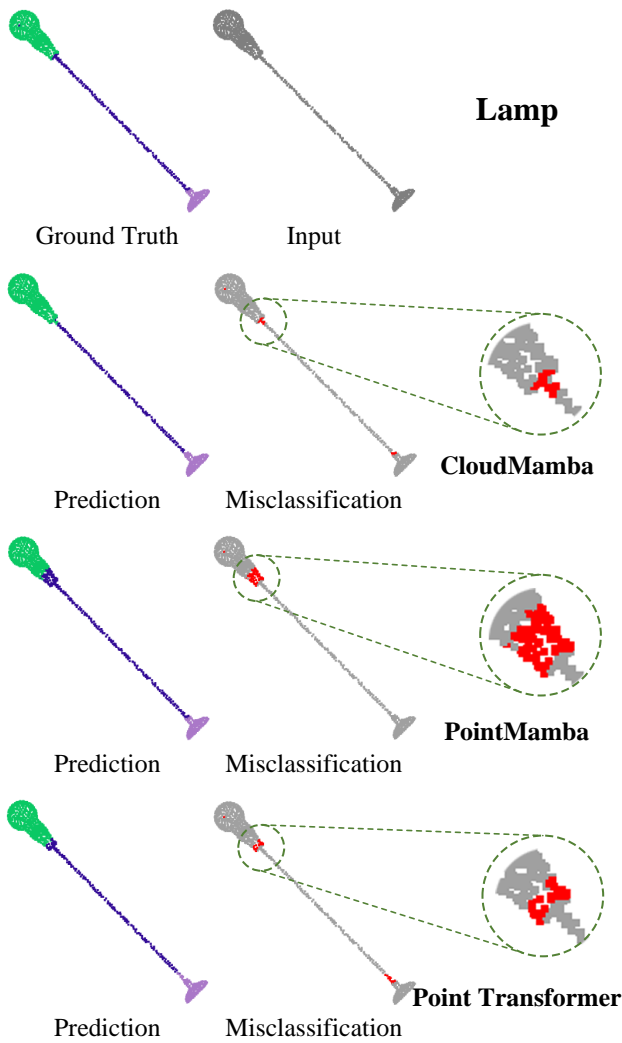
Transformer (Zhao et al. 2021) on ShapeNet dataset, which reveals that our network is able to achieve better segmentation results at the boundary of objects. For ModelNet40, ScanObjectNN, and S3DIS datasets, most of the works does not report the accuracy for each category. To clearly demonstrate CloudMamba’s performance in each category, as well

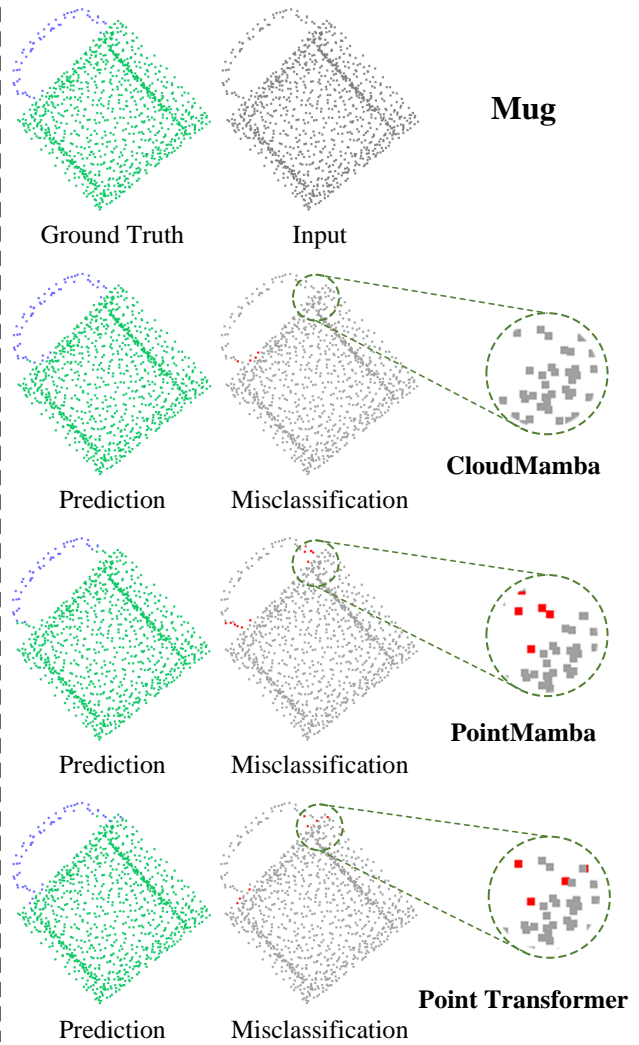
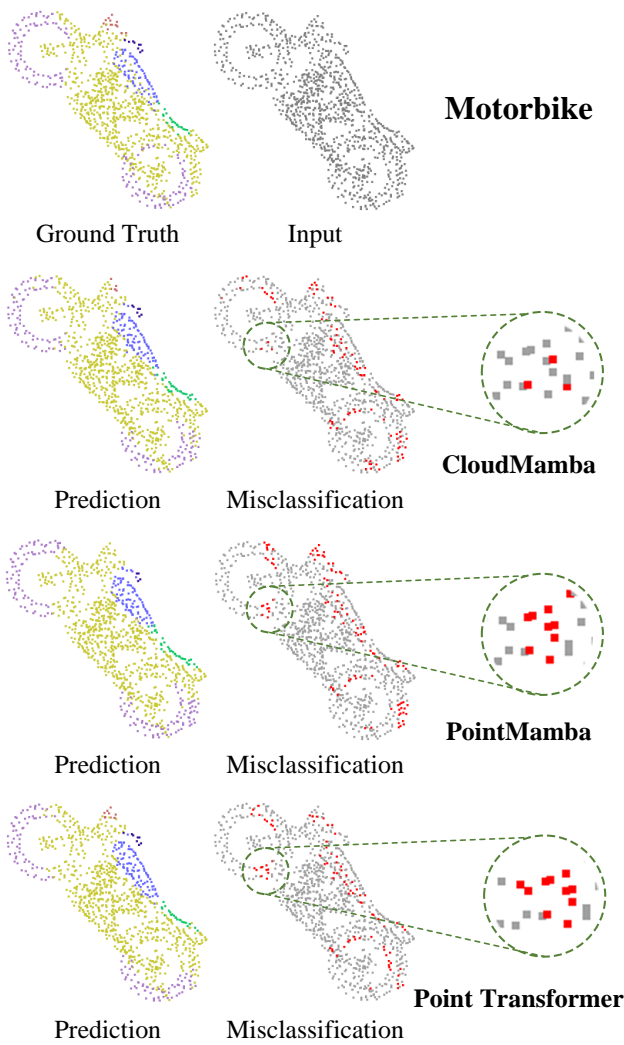
as to facilitate subsequent studies, Tab. 10, Tab. 11, and Tab. 12 list the accuracy of our network for each category on ModelNet40, ScanObjectNN, and S3DIS datasets, respectively. Furthermore, we visualize the segmentation results of CloudMamba for different scenarios in S3DIS dataset, as shown in Fig. 8.

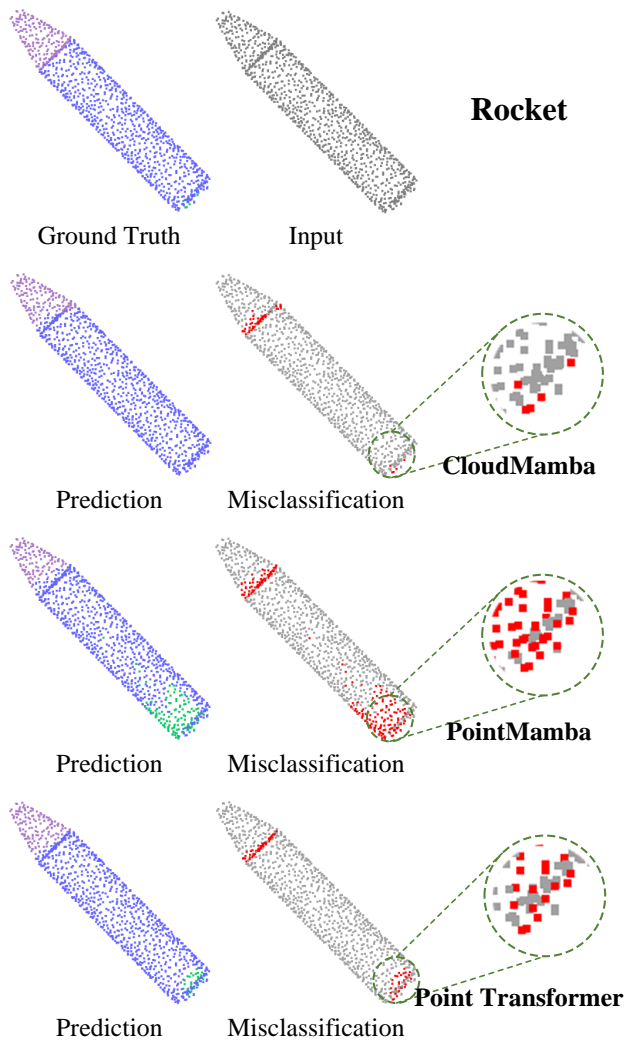
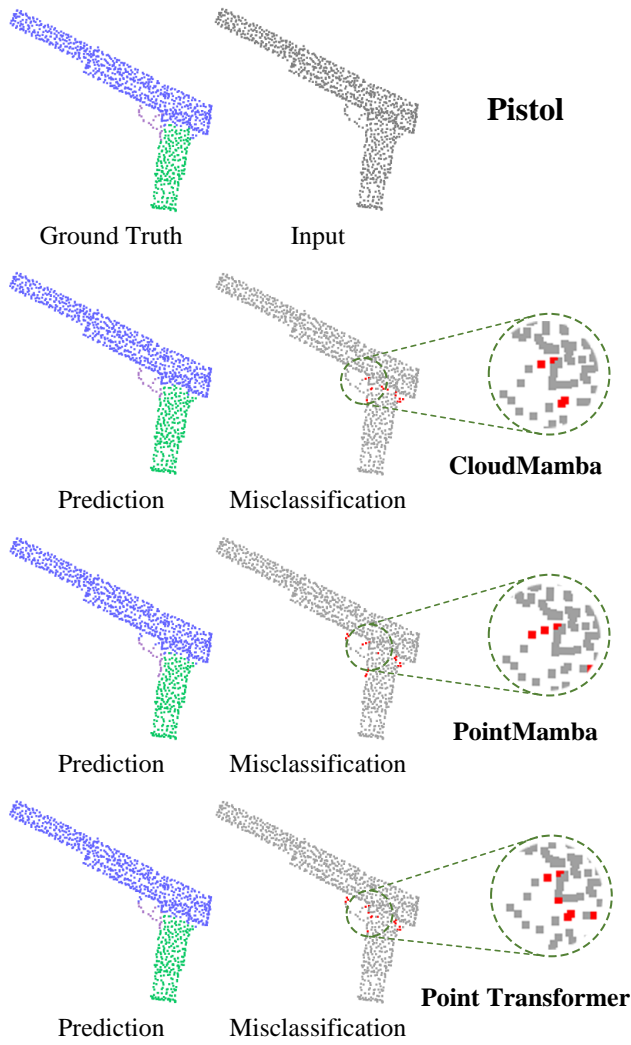












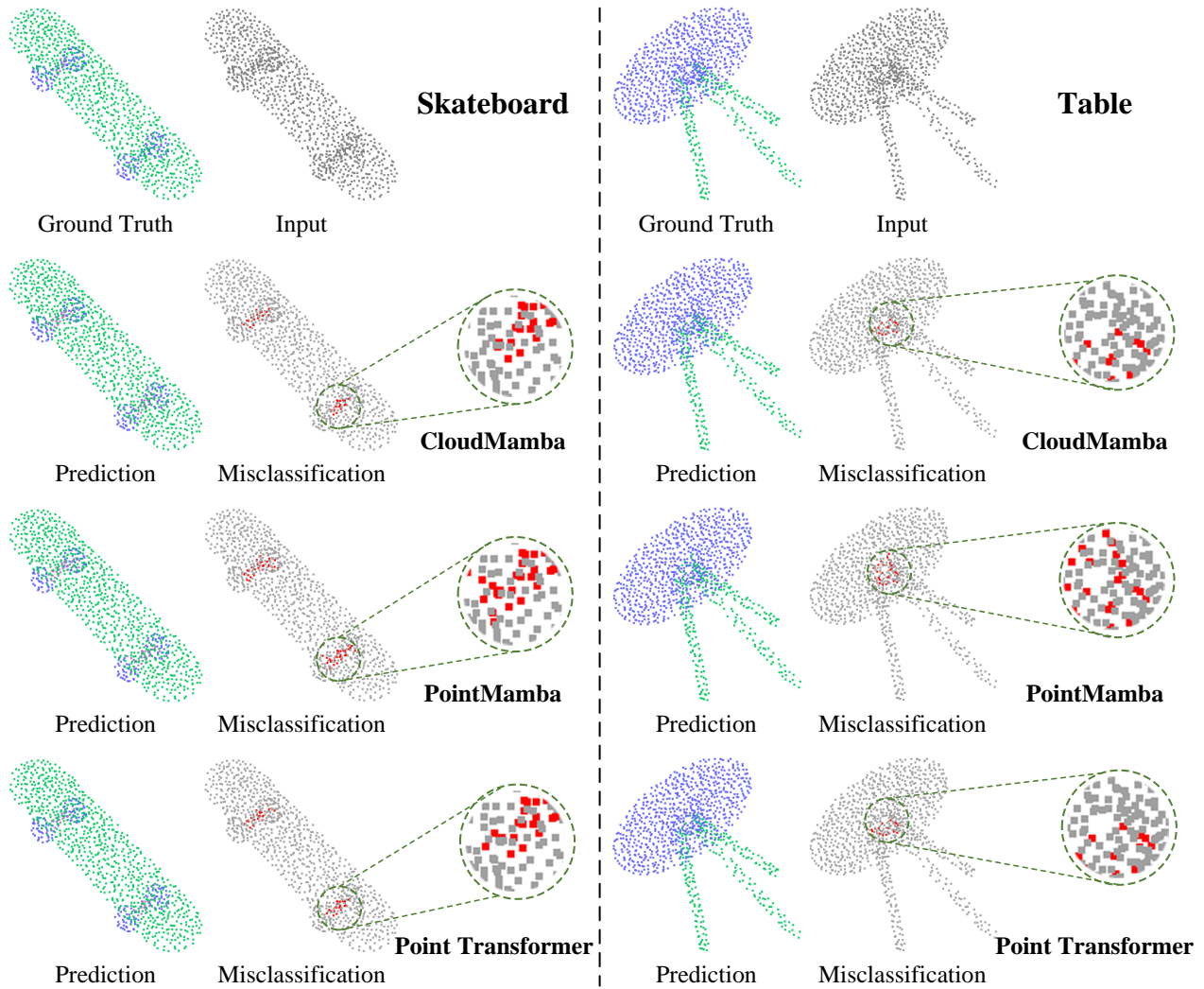
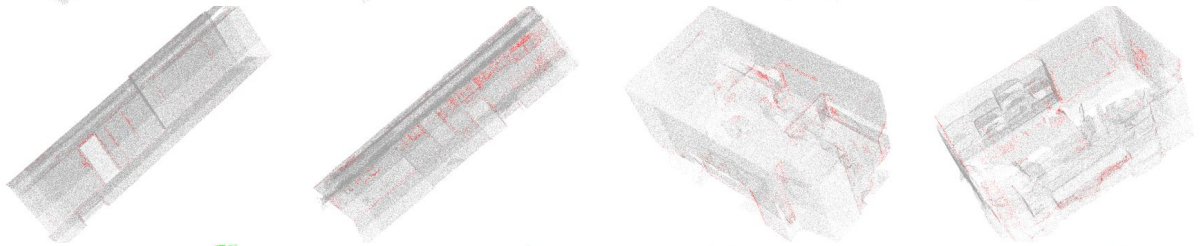


Figure 7: Qualitative results of CloudMamba, PointMamba, and Point Transformer on each category in ShapeNet dataset.

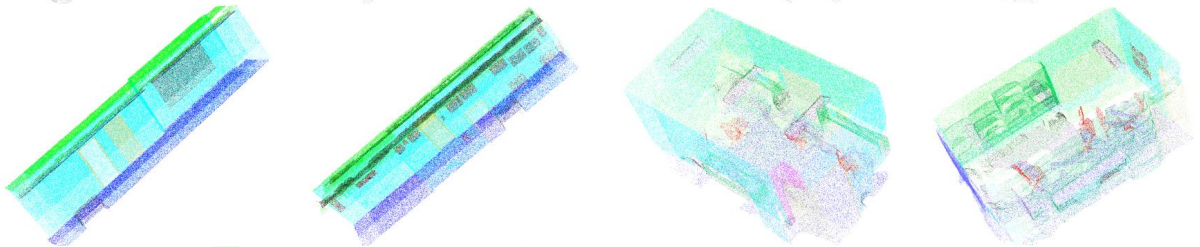
Input



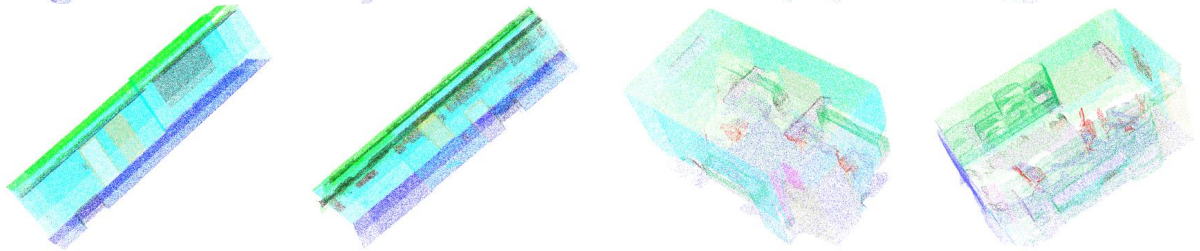
Error Points



Ground Truth



Prediction



Ceiling Floor Wall Beam Column Sofa Window Door Table Chair Bookcase Board Clutter



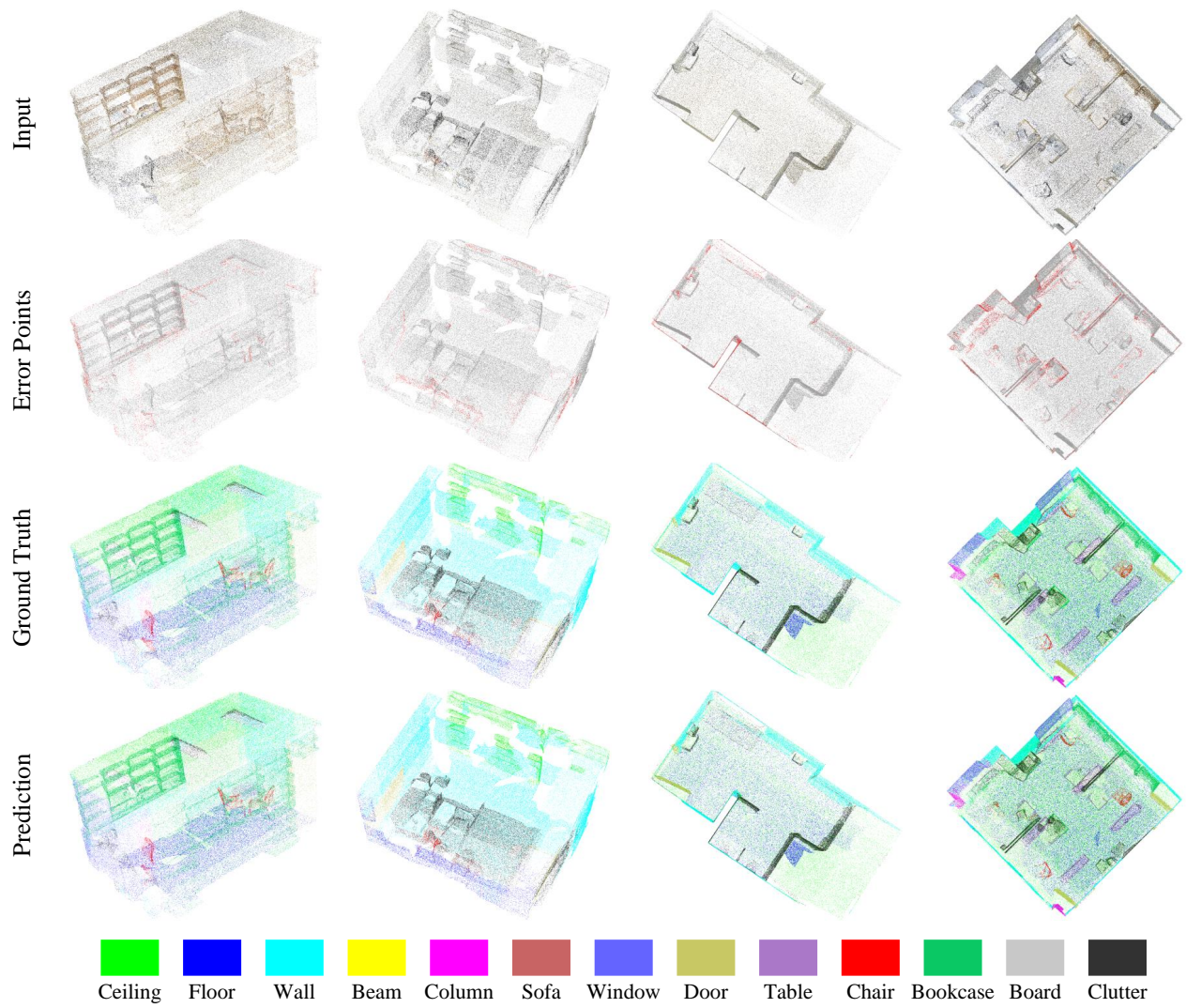


Figure 8: Qualitative results of CloudMamba on different scenarios in S3DIS dataset.